



IDENTIFICATION AND CLASSIFICATION OF BEAM LOSS PATTERNS IN THE LARGE HADRON COLLIDER

Panagiotis Theodoropoulos

Supervisors (CERN)

Gianluca Valentino

Stefano Redaelli

Supervisor (UCL)

Mark Herbster

This report is submitted as part requirement for the MSc Machine Learning at University College London. It is substantially the result of my own work except where explicitly indicated in the text.

The report may be freely copied and distributed provided the source is explicitly acknowledged (CERN-THESIS-2015-128)

September 2015

Abstract

The Large Hadron Collider, is the largest particle accelerator ever built, achieving record beam energy and beam intensity. Beam losses are unavoidable and can risk the safety of accelerator's components. Beam loss maps are used to validate the collimation system, designed to protect the accelerator against beam losses. The complexity of this system requires well defined inspection methods and well defined case studies that ensure normal operation and efficient performance evaluation. In this work, enhancements are proposed to the existing validation methods, demonstrating that with a low-rank approximation of the beam loss data sets, a robust visualization of the beam loss patterns is obtained in lower dimensional spaces, that can then be used to train a classifier, a step towards automating the inspection mechanisms.

Acknowledgments

I would like to thank Stefano Redaelli for providing me the opportunity to pursue the current research project at collimation team at CERN and Gianluca Valentino for defining the research topic and the thorough discussions on the emerged researched case studies. I would like to thank Roderik Bruce for the very elaborate discussions on collimation configurations studies, concluding to beam dynamics interpretations. I would like also to thank all collimation team mates for their collaboration during shifts at Cern Control Centre (CCC). I would like to thank Mark Herbster for the academic freedom provided during my studies, which allowed me to experiment many different ideas and implementations before concluding to the reported ones, as well as his detailed comments on the concluded methods and results of the thesis.

Contents

| | | |
|----------|--|-----------|
| 1 | Introduction | 1 |
| 2 | Machine Learning | 2 |
| 2.1 | Learning Theory | 2 |
| 2.2 | Support Vector Machines | 4 |
| 2.2.1 | Problem formulation | 4 |
| 2.2.2 | Soft Margin SVM | 6 |
| 2.2.3 | Geometric approach | 7 |
| 2.3 | Singular Value Decomposition | 11 |
| 2.3.1 | Geometric interpretation | 12 |
| 2.4 | Principal Component Analysis | 13 |
| 3 | The Large Hadron Collider | 15 |
| 3.1 | Overview | 15 |
| 3.2 | Collimation system | 17 |
| 3.2.1 | Purpose | 17 |
| 3.2.2 | Jaw movement | 18 |
| 3.2.3 | Half gaps | 19 |
| 3.3 | Beam Loss Monitors | 21 |
| 4 | Learning from Beam Loss Monitors | 25 |
| 4.1 | Requirements | 25 |
| 4.2 | BLM selection | 26 |
| 4.3 | Data organization | 28 |
| 4.4 | Feature extraction | 29 |
| 4.5 | Identification of beam loss patterns | 32 |
| 4.5.1 | Major collimator setting changes | 32 |
| 4.5.2 | Minor collimator setting changes | 35 |
| 4.5.3 | Proton - Ion beams | 39 |
| 4.6 | Classification of beam loss patterns | 41 |
| 4.6.1 | Implementation scheme | 42 |
| 4.6.2 | Model assessment | 43 |
| 4.6.3 | Classification results | 44 |
| 5 | Conclusion | 52 |
| | References | 53 |
| 6 | Appendix | 54 |
| 6.1 | Accelerator Physics | 54 |
| 6.1.1 | Particle acceleration | 54 |
| 6.1.2 | Particle motion | 54 |
| 6.1.3 | Beam scraping | 55 |

| | | |
|-----|---------------------|----|
| 6.2 | BLM lists | 55 |
|-----|---------------------|----|

List of Figures

| | | |
|----|--|----|
| 1 | two candidate hyperplanes | 4 |
| 2 | embedding in feature space | 6 |
| 3 | convex hulls defining SVM classes [12] | 9 |
| 4 | progressive evolution of convex hull [12] | 10 |
| 5 | geometric interpretation of least squares for $l=2$ | 12 |
| 6 | LHC map [14] | 15 |
| 7 | an LHC collimator [14] | 17 |
| 8 | collimation hierarchy showing the nominal settings in units of beam sigma [14] | 18 |
| 9 | design of a collimator [14] | 18 |
| 10 | LVDT working principle [11] | 19 |
| 11 | uncovered Ionization Chamber [14] | 21 |
| 12 | Beam Loss Monitor attached on a focusing quadrupole [14] | 21 |
| 13 | loss map on B2VER (IR 1-8) | 22 |
| 14 | beam loss map on B1VER zoomed in IR7 | 22 |
| 15 | collimation loss map on B1VER - zoomed in IR7 | 23 |
| 16 | analytic collimation loss map on B1VER - zoomed in IR7 | 24 |
| 17 | example of an extracted dataset for one case study (Beam/Plane/Energy) . . | 28 |
| 18 | orthogonal projections | 30 |
| 19 | eigenvalue decay at 450 GeV | 31 |
| 20 | broken hierarchy on B2VER loss map at 4000 GeV | 32 |
| 21 | normal hierarchy on B2VER loss map at 4000 GeV | 33 |
| 22 | beam loss map B2VER patterns at 4000GeV.png | 34 |
| 23 | beam loss patterns for B1HOR Injection events | 36 |
| 24 | beam loss patterns for B1VER Injection events.png | 36 |
| 25 | beam loss patterns for B2HOR Injection events.png | 37 |
| 26 | beam loss patterns for B2VER Injection events.png | 37 |
| 27 | B1HOR proton-ion loss patterns | 39 |
| 28 | B1VER proton-ion loss patterns | 39 |
| 29 | implementation scheme (flowchart) | 42 |
| 30 | 5-fold cross validation on $\hat{\mathbf{X}}$ | 43 |
| 31 | B1HOR450 | 44 |
| 32 | B1VER450 | 46 |
| 33 | B2HOR450 | 48 |
| 34 | B2VER450 | 50 |

List of Tables

| | | |
|----|---|----|
| 1 | LHC specification | 16 |
| 2 | collimator settings | 20 |
| 3 | blm naming conventions | 23 |
| 4 | collimator naming conventions | 23 |
| 5 | eigenvalue percentages | 31 |
| 6 | beam losses in magnet Q8 in DS | 33 |
| 7 | TCLA.A6L7.B2 alignment for broken and normal hierarchy (upstream) . . . | 33 |
| 8 | TCLA.A6L7.B2 alignment for broken and normal hierarchy (downstream) . . | 33 |
| 9 | B2VER4000 | 34 |
| 10 | jaw midpoint shifts (2015 test) | 35 |
| 11 | UTC timestamps for proton beam loss maps at 450 GeV | 38 |
| 12 | proton - ion B1 loss maps combined | 40 |
| 13 | confusion matrix B1HOR450 (linear, rbf kernel) | 44 |
| 14 | abnormal B1HOR450 loss maps | 45 |
| 15 | confusion matrix B1VER450 (linear kernel) | 46 |
| 16 | confusion matrix B1VER450 (rbf kernel) | 46 |
| 17 | abnormal B1VER450 loss maps | 47 |
| 18 | confusion matrix B2HOR450 (linear, rbf kernel) | 48 |
| 19 | abnormal B2HOR450 loss maps | 49 |
| 20 | confusion matrix B2VER450 (linear, rbf kernel) | 50 |
| 21 | abnormal B2VER450 loss maps | 51 |
| 22 | beam scraping [5] | 55 |
| 23 | BLM setup 1 | 56 |
| 24 | BLM setup 2 | 57 |
| 25 | BLM setup 3 | 58 |
| 26 | BLM setup 4 | 59 |
| 27 | BLM subset selection | 60 |

Acronyms

| | |
|-------|---|
| ALICE | A Large Ion Collider Experiment |
| ATLAS | A Toroidal LHC ApparatuS |
| BLM | Beam Loss Monitor |
| B1 | Beam one |
| B2 | Beam two |
| CCC | Cern Control Center |
| CD | Center Downstream |
| CMS | Compact Myon Solenoid |
| CU | Center Upstream |
| HOR | Horizontal plane |
| IP | Interaction Point |
| IR | Interaction Region |
| IC | Ionization Chamber |
| KLT | Karhunen-Loève Transform |
| LD | Left Downstream |
| LHC | Large Hadron Collider |
| LHCb | Large Hadron Collider beauty |
| LU | Left Upstream |
| LVDT | Linear Variable Differential Transformer |
| LIC | Little Ionization Chamber |
| MSE | Mean Square Error |
| PCA | Principal Component Analysis |
| RBF | Radial Basis Function |
| RD | Right Downstream |
| RF | Radio Frequency |
| RKHS | Reproducing Kernel Hilbert Spaces |
| RU | Right Upstream |
| SVD | Singular Value Decomposition |
| SC | Super Conducting |
| SVM | Support Vector Machines |
| TCHSV | Target Collimator Halo Scraper Vertical |
| TCHSH | Target Collimator Halo Scraper Horizontal |
| TCHSS | Target Collimator Halo Scraper Skew |
| TCLD | Target Collimator Long Dispersion |
| TCLA | Target Collimator Long Absorber |
| TCP | Target Collimator Primary |
| TCSG | Target Collimator Secondary Graphite |
| TCSM | Target Collimator Secondary Metallic |
| TCT | Target Collimator Tertiary |
| VC | Vapnik-Chervoneskis |
| VER | Vertical plane |

1 Introduction

The scope of this thesis is to study and evaluate current validation methods performed at collimation project at CERN data sets maintained within the collimation project at CERN and their potential for use during infrequent validation campaigns that inspect the configuration of the LHC collimation system. The importance of this study is to offer an alternative approach for visualizing the beam loss patterns and deciding whether they are consistent or not (normal or abnormal), given a certain configuration of the LHC collimation system.

The study was structured in several levels, involving at first development of information retrieval tools dedicated for organization of data for the goals of the thesis. Pre-processing, visualization, cycles of readings of the associated material and final interpretation. Study of materials in statistical learning theory and multivariate analysis to evaluate the usage of the candidate methods and final decision. The described and utilized methods derived from quantitative research for several decades or even hundreds of years. In this thesis they have been encapsulated under the term *Machine Learning*, which is currently used as an umbrella term to refer to these methods.

From the field of Multivariate Methods, in particular Principal Component Analysis (PCA) was implemented in order to extract features from organized and physically pre-processed multi-dimensional beam loss datasets, for usable visualization of beam loss patterns for the practical purposes of this thesis. What is shown in this thesis is that the information stored in data from Beam Loss Monitors, when filtered carefully and organized in case studies - in order to reflect the occurrence of beam loss patterns at a certain beam mode configuration (and thus a certain LHC collimator configuration) - can be retained at a high level of accuracy when reducing the dimensionality of the corresponding filtered data sets. Then, the transformed data sets can be used for learning statistically the discovered patterns in lower dimensional spaces, through the use of Support Vectors Machines (SVMs), classifying the identified patterns, or else deciding whether the patterns are normal or abnormal.

The thesis was formed in three main chapters. The second chapter, elaborates on how statistical learning theory generally approaches a learning problem followed from the formal description of Support Vector Machines (SVMs), which have been built based on the previous described principles (applied in this work for *classification* purposes). Multivariate methods are discussed as they have been used for pattern identification purposes, discussing also the eigenvalue problem and its connection to the used methods. The third chapter introduces the LHC collimation system, its purpose and main functionality. Standard data analysis performed within collimation is elaborated providing accelerator physics justifications, outlining the objectives of the analysis and how it tailored decisions - such as the choice of beam loss monitors - for the final extraction of the input data sets. The application of the proposed implementation scheme is presented in the fourth chapter concluding the final results.

2 Machine Learning

2.1 Learning Theory

In statistical learning a *source* is assumed to generate samples from a distribution that is not known. A *learner* observes the generated data and tries to understand the source by identifying patterns. A learner can then build a system, which based on the identified patterns, can make predictions on the new data points generated from the source. An additional assumption that is made is that the data points being generated are *independently and identically distributed* (i.i.d), meaning that the occurrence of a new data point is not related to the ones already emitted, yielding maximum information each time. In this study, the same assumptions will be admitted, assuming that an *event* is not related to the others, where each event leaves a footprint or a pattern, which we want to identify.

This learning principle can be challenged in many different ways. For instance the patterns being detected have to be *stable*, not becoming distorted when increasing significantly the number of data points. Thus, the space being explored has to be sufficiently *robust*, in order to be confident that the patterns are indeed stable. In practical applications when data entries have to be filtered under certain criteria or requirements, may restrict the resulting sample size that we would like to learn from. This will be encountered later in the later part of the thesis.

Thinking that each data point arrives from a set of random variables, which follow arbitrary distributions, then when sending the number of random variables to infinity the overall distribution of generated data points is said to be normal [7]. Motivated by this, a usual decision is to assume that the unknown distribution related to the source is a Gaussian one. The need to introduce assumptions is a natural consequence of the *no free lunch theorem*, namely that generalization needs not only data, but also knowledge, for which only assumptions can be made. Hence, it is very common to see traditional pattern recognition algorithms being bench-marked based on gaussian samples. The question is how such methods can be adapted on real, noisy data where no direct assumptions can be made for the explored space, which is the case and challenge of this study.

The above consist main challenges of *inference* and in the scope of this thesis we will be concerned with *inductive* inference, summarized as follows:

- identify a phenomenon
- construct model from phenomenon
- make predictions based on the inferred model

To formalize the learning problem we define the input space X and output space Y . The goal is to find the predictive function g which predicts Y from X . Let H denote the hypothesis space containing the prediction rules. Now, keeping fixed the inference rule that selects the hypothesis h_S the generalization error is expressed as follows:

$$err_{\mathcal{D}}(h_S) = \mathcal{D}\{(\mathbf{x}, y) : h_S(\mathbf{x}) \neq y\}$$

Where \mathcal{D} is the unknown distribution generating the *test samples*, which is dependent on the selection of the *training samples*. In practice the expected/test error is used as a *proxy*, which is the measured error, when evaluating learning models. In this thesis the evaluation incorporates the cross-validatory choice, where the main idea is to create many hypotheses based on the groups of training samples and then validate the hypotheses, which are then used for testing.

2.2 Support Vector Machines

Support Vector Machines (SVMs) were pioneered by Vladimir Vapnik in 1963 [20]. Given some observations, with *no specific assumptions on their distribution*, which is considered unknown, *yet fixed*, based on the Vapnik-Chervoneskis (VC) - theory, the best possible separation is sought, which discriminates the observations in two groups. SVMs use a hypothesis space of linear functions defined in a feature space, *trained* through optimizing a model dependent on the training samples. Then when embedding future observations in the feature space, the produced model is used to classify them to groups. The process of classifying future observations based on the inferred model can be found being mentioned as *prediction* and the groups being mentioned as *classes*. The above require the hypothesis space not to evolve nor degrade (remain constant) at prediction.

Let $\mathbf{x}_i, i = 1, 2, \dots, N$ be the feature vectors of the training set \mathbf{X} . These vectors are members of two possible classes c_1, c_2 .

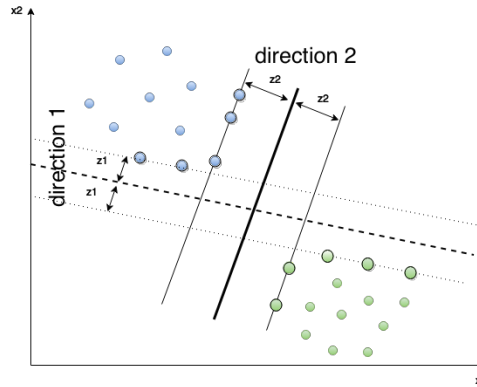


Figure 1: two candidate hyperplanes

Given the example in Figure 1, we would select the hyperplane following the second direction for separating the two classes. The reason is that it provides the best separation between the two classes, reducing the chance of mis-classifying a testing vector to the wrong class. This is related to the generalization problem referred in the learning theory section. Now that we have built the motivation for finding the best possible hyperplane we are ready to build the mathematical requirements that will lead us to the solution of this problem.

2.2.1 Problem formulation

The hyperplane is defined from its direction and its position in the space. We will use the term *margin* to refer to the gap between the two classes and the hyperplane. The hyperplane as we define it belongs to the family of *linear discriminant functions*.

$$g(\mathbf{x}) = \mathbf{w}^T \mathbf{x} + b = 0$$

where $\mathbf{w} = [w_1, w_2, \dots, w_l]^T$ is the weight vector and b is the threshold or bias.

Since our goal is to maximize the separation distance, the margin has to be maximized. The margin totals $\frac{1}{\|w\|} + \frac{1}{\|w\|} = \frac{2}{\|w\|}$, where for each class:

$$\begin{aligned}\mathbf{w}^T \mathbf{x} + b &\geq 1 \quad \forall x \in c_1 \\ \mathbf{w}^T \mathbf{x} + b &\leq -1 \quad \forall x \in c_2\end{aligned}$$

Thus, the optimization problem is formulated as follows:

$$\begin{aligned}\min \left\{ \frac{1}{2} \mathbf{w}^T \mathbf{w} \right\} \text{ subject to } y_i(\mathbf{w}^T \mathbf{x}_i + b) &\geq 1 \text{ for } i = 1, \dots, m \\ \min \left\{ \frac{1}{2} \mathbf{w}^T \mathbf{w} \right\} \text{ subject to } y_i(\mathbf{w}^T \mathbf{x}_i + b) - 1 &\geq 0 \text{ for } i = 1, \dots, m\end{aligned}$$

Looking for the minimization of the norm - thus maximizing the margin (*max-margin SVM*) - subject to the introduced constraints. Hence, the *primal* form of the Lagrangian can be formulated as follows, introducing α_i Lagrange multipliers, subject to the constraints:

$$\mathcal{L}_p = \frac{1}{2} \mathbf{w}^T \mathbf{w} - \sum_{i=1}^m \alpha_i [y_i(\mathbf{w}^T \mathbf{x}_i + b) - 1], \quad \alpha_i \geq 0$$

$$\mathcal{L}_p = \frac{1}{2} \|\mathbf{w}\|^2 - \sum_{i=1}^m \alpha_i [y_i(\mathbf{w}^T \mathbf{x}_i + b) - 1], \quad \alpha_i \geq 0$$

$$\frac{\partial \mathcal{L}_p}{\partial \mathbf{w}} = \frac{1}{2} \cdot 2 \cdot \mathbf{w} - \sum_{i=1}^m \alpha_i \cdot y_i \cdot 1 \cdot \mathbf{x}_i = 0, \quad \alpha_i \geq 0$$

$$\mathbf{w} = \sum_{i=1}^m \alpha_i y_i \mathbf{x}_i$$

$$\frac{\partial \mathcal{L}_p}{\partial b} = \sum_{i=1}^m \alpha_i y_i = 0$$

substituting now the linear combination found by optimizing the primal, we retrieve the *dual* form:

$$\mathcal{L}_d = \frac{1}{2} \sum_{i=1}^m \sum_{j=1}^m \alpha_i \alpha_j y_i y_j \langle \mathbf{x}_i, \mathbf{x}_j \rangle - \sum_{i=1}^m \sum_{j=1}^m \alpha_i \alpha_j y_i y_j \langle \mathbf{x}_i, \mathbf{x}_j \rangle + \sum_{i=1}^m \alpha_i$$

$$\mathcal{L}_d = \sum_{i=1}^m \alpha_i - \frac{1}{2} \sum_{i=1}^m \sum_{j=1}^m \alpha_i \alpha_j y_i y_j \langle \mathbf{x}_i, \mathbf{x}_j \rangle$$

In the dual form we have decoupled the inner product which is based on the training input, which can be replaced with a kernel function. This is the *kernel trick*.

The kernel trick is useful when working with training data, where the existing structure is not always a linear function of the data representation. In these cases an approach is needed for learning non-linear models. One way is based on the Reproduced Kernel Hilbert spaces (RKHS), where the main idea is to map the input variables into a new space, such that the nonlinear task is transformed into a linear one. Thus, a kernel method can be used in order to map data points within higher dimensional spaces. The dimension can be even infinite and thus not practical to work with the mapped data explicitly. This transition is denoted as follows:

$$\phi : x \in \mathcal{R}^n \longrightarrow \phi(\mathbf{x}) \in F \subseteq \mathcal{R}^{\mathcal{N}}$$

The chosen feature map ϕ re-codes the original dataset from $\mathbf{X} = \{(x_1, y_1), \dots, (x_l, y_l)\}$ to $\hat{\mathbf{X}} = \{(\phi(x_1), y_1), \dots, (\phi(x_l), y_l)\}$. The kernel function is defined as follows:

$$k(\mathbf{x}, \mathbf{y}) = \langle \phi(\mathbf{x}), \phi(\mathbf{y}) \rangle = \phi(\mathbf{x})^T \phi(\mathbf{y})$$

Thus:

$$\mathcal{L}_d = \sum_{i=1}^m \alpha_i - \frac{1}{2} \sum_{i=1}^m \sum_{j=1}^m \alpha_i \alpha_j y_i y_j k(\mathbf{x}_i, \mathbf{x}_j)$$

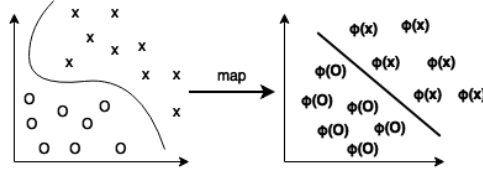


Figure 2: embedding in feature space

2.2.2 Soft Margin SVM

At certain classification problems it is often the case that patterns very close to the decision boundary, violate the constrain $y_i(\mathbf{w}^T \mathbf{x}_i + b) \geq 1$ and being mis-classified. Then we wish to have a way to manipulate the margin so as to learn such difficult patterns. This can be done by relaxing the constrains, introducing the so-called *slack variables* $\xi_i \geq 0$. Modifying the constrain to $y_i(\mathbf{w}^T \mathbf{x}_i + b) \geq 1 - \xi_i$. This is the *soft margin SVM* [6] formalized as follows:

$$\min \left\{ \frac{1}{2} \mathbf{w}^T \mathbf{w} + C \sum_{i=1}^m \xi_i^2 \right\} \text{ subject to } y_i(\mathbf{w}^T \mathbf{x}_i + b) \geq 1 - \xi_i \text{ for } \xi_i \geq 0, i = 1, \dots, m$$

With the parameter C controls the trade-off of the margin maximization between the minimization of the training error. Can be seen as a *regularizer*, which can also be found being called as *penalty factor*.

Now, the primal form incorporating slack variables is written as follows:

$$\mathcal{L}_p = \frac{1}{2} \mathbf{w}^T \mathbf{w} + \frac{1}{2} C \sum_{i=1}^m \xi_i^2 - \sum_{i=1}^m \alpha_i [y_i (\mathbf{w}^T \mathbf{x}_i + b) - 1 + \xi_i], \quad 0 \leq \alpha_i \leq C, i = 1, \dots, m$$

Where the parameter C is the penalty factor, expressing the control of the contribution of the slack variables ξ_i .

$$\frac{\partial L_p}{\partial \mathbf{w}} = 2 \cdot \frac{1}{2} \cdot \mathbf{w} + 0 - \sum_{i=1}^m \alpha_i \cdot y_i \cdot \mathbf{x}_i = 0 \rightarrow \mathbf{w} = \sum_{i=1}^m \alpha_i y_i \mathbf{x}_i, \quad \alpha_i \geq 0$$

$$\frac{\partial L_p}{\partial b} = \sum_{i=1}^m \alpha_i y_i = 0$$

Optimizing also with respect to ξ :

$$\frac{\partial L_p}{\partial \xi} = C \xi - \alpha$$

Substituting the relations obtained after the optimization of \mathcal{L}_p we retrieve:

$$\mathcal{L}_d = \sum_{i=1}^m \alpha_i - \frac{1}{2} \sum_{i=1}^m \sum_{j=1}^m \alpha_i \alpha_j y_i y_j \langle \mathbf{x}_i, \mathbf{x}_j \rangle - \frac{1}{2} C \langle \boldsymbol{\alpha} \cdot \boldsymbol{\alpha} \rangle$$

This version of SVM will be used later for classifying the identified patterns, evaluating the model through cross validation, finding the best parameters C (penalty factor) and γ , controlling the radius when the Radial Basis Function kernel is chosen.

$$\mathcal{L}_d = \sum_{i=1}^m \alpha_i - \frac{1}{2} \sum_{i=1}^m \sum_{j=1}^m \alpha_i \alpha_j y_i y_j k(\mathbf{x}_i, \mathbf{x}_j) - \frac{1}{2} C \langle \boldsymbol{\alpha} \cdot \boldsymbol{\alpha} \rangle$$

SVMs have been also approached from a different perspective, based on the observation that the resulting optimization problem is connected to the optimization problem for finding a convex hull. The connection will be briefly reported in the next section [12] [18].

2.2.3 Geometric approach

In this section a geometrical interpretation of the Support Vector Machine classifier is presented [12]. The intuitive description will be based on the notion of geometric sets in geometry. In particular convex hulls, and thus we will remind briefly the general principle underlying them. We distinguish between two cases, when the classes are *separable* and when they are *overlapping*.

- Separable Classes

Assuming a set \mathbf{X} defined in a Euclidean space. A convex hull or convex envelope of points in that space is the smallest convex set that contain the elements of \mathbf{X} . In other words a convex hull of finite point set S is the set of all convex combinations of its points. In a convex combination, each \mathbf{x}_i in S is assigned a weight or coefficient a_i in such a way that the coefficients are all non-negative and sum to one. These weights are used to compute a weighted average of the points. For each choice of coefficients, the resulting convex combination is a point in the convex hull and the whole convex hull can be formed by choosing coefficients in all possible ways. Thus, formally we can express the convex hull as follows:

$$\text{conv}X = \left\{ \mathbf{y} : \mathbf{y} = \sum_{i=1}^{|S|} \alpha_i \mathbf{x}_i \mid \sum_{i=1}^{|S|} \alpha_i = 1, i = 1, 2, \dots, |S|, 0 \leq \alpha_i \leq 1 \right\}$$

We will denote the symbol X^+ define the set of the points belonging in the first class and X^- the set of points belonging to the second class. Hence $S = X^+ \cup X^-$. Since every point in the convex hull of a set is a convex combination of all the points of the set, it is evident that finding the closest points between the two convex hulls, $\text{conv}X^+$ and $\text{conv}X^-$ is equivalent to solving the optimization task given by:

$$\begin{aligned} \min_{\alpha} & \left\| \sum_{i:y_i=1} \alpha_i \mathbf{x}_i - \sum_{i:y_i=-1} \alpha_i \mathbf{x}_i \right\|^2 \\ & \sum_{i:y_i=1} \alpha_i = 1 \\ & \sum_{i:y_i=-1} \alpha_i = 1 \end{aligned}$$

for $i = 1, 2, \dots, N$

The constraints set by the coefficients α_i respect the convexity conditions for each of the two classes. It turns out that the optimization problem can be written as:

$$\begin{aligned} & \text{minimize} \sum_{i,j} y_i y_j \alpha_i \alpha_j \mathbf{x}_i^T \mathbf{x}_j \\ & \text{subject to} \sum_{i=1}^N y_i \alpha_i = 0 \\ & \sum_{i=1}^N \alpha_i = 2 \\ & \alpha_i \geq 0, i = 1, 2, \dots, N \end{aligned}$$

- Overlapping Classes

The previous geometric interpretation was valid for separable classes. For non-separable classes we must reconsider the geometric interpretation due to the fact that the minimum

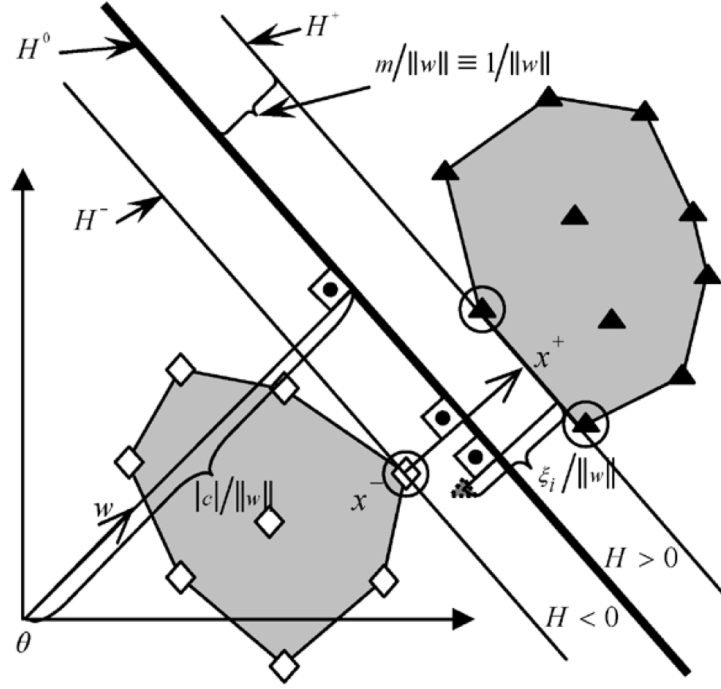


Figure 3: convex hulls defining SVM classes [12]

distance points coincide. Instead, the reduced convex hull of a vector set X , denoted by $R(X, \mu)$ is defined as follows:

$$R(X, \mu) = \left\{ \mathbf{y} : \mathbf{y} = \sum_{i=1}^N \alpha_i \mathbf{x}_i, \mathbf{x}_i \in \mathbf{X}, \sum_{i=1}^N \alpha_i = 1, 0 \leq \alpha_i \leq \mu, i = 1, 2, \dots, N \right\}$$

The difference with the separable geometric interpretation is that the coefficients α are restricted to be less or equal to $\mu < 1$ instead of 1. It is straightforward to see that $R(X, \mu) \subseteq \text{conv}X$. The convex hulls of two overlapping classes together with the respective reduced convex hulls, for different values of μ , are illustrated in Figure 4, demonstrating the effect of the convex hull size when adjusting μ .

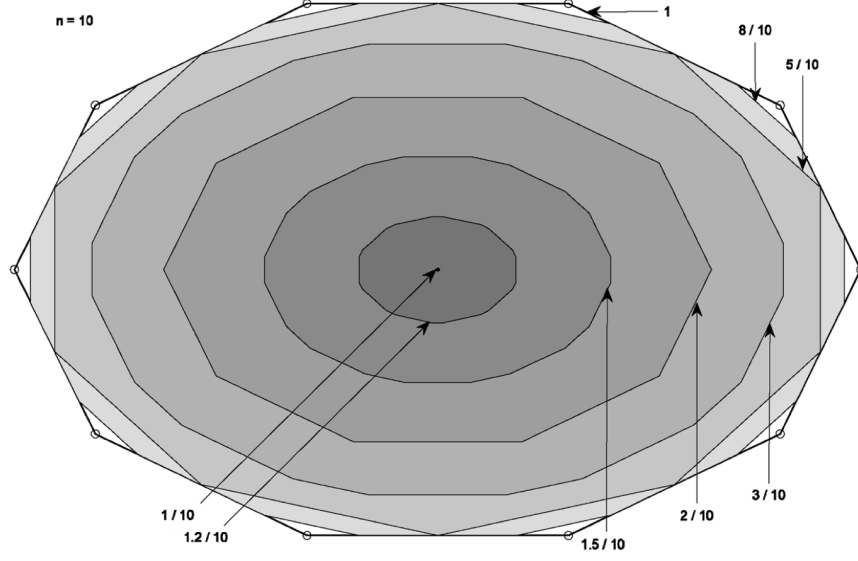


Figure 4: progressive evolution of convex hull [12]

The separability of convex hulls for different values of μ is achieved for a certain threshold of μ . Thus, by selecting the value of μ the respective reduced convex hulls of the two classes become separable and then try to find the nearest points between them. The nearest points can be found through the following optimization problem:

$$\begin{aligned}
 & \text{minimize } \sum_{i,j} y_i y_j \alpha_i \alpha_j \mathbf{x}_i^T \mathbf{x}_j \\
 & \text{subject to } \sum_{i=1}^N y_i \alpha_i = 0, \sum_{i=1}^N \alpha_i = 2 \\
 & 0 \leq \alpha_i \leq \mu, i = 1, 2, \dots, N
 \end{aligned}$$

This is the Wolfe dual formulation of modified version of SVM given by:

$$\begin{aligned}
 \min J(\mathbf{w}, \mathbf{w}_0, \boldsymbol{\xi}, \rho) &= \frac{1}{2} \|\mathbf{w}\|^2 - 2\rho + \mu \sum_{i=1}^N \xi_i \\
 \text{subject to } y_i [\mathbf{w}^T \mathbf{x}_i + \mathbf{w}_0] &\geq \rho - \xi_i \\
 \xi_i &\geq 0, \rho \geq 0, i = 1, \dots, N
 \end{aligned}$$

2.3 Singular Value Decomposition

The Singular Value Decomposition (SVD) is a linear algebra method which given an $\mathbf{X}^{m \times l}$ matrix of rank $r \leq \min\{m, l\}$ (allowing also not to be necessarily full), there exist unitary matrices $\mathbf{U}^{m \times r}$ and $\mathbf{V}^{r \times l}$ for which the following expression is true:

$$\mathbf{X}^{m \times l} = \mathbf{U}^{m \times r} \mathbf{D}^{r \times r} (\mathbf{V}^T)^{r \times l}$$

where

$$\mathbf{U}_r := [\mathbf{u}_1, \dots, \mathbf{u}_r] \in R^{m \times r}, \mathbf{V}_r := [\mathbf{v}_1, \dots, \mathbf{v}_r] \in R^{l \times r}$$

This task essentially orthogonalizes the column space of \mathbf{X} . The matrix $\mathbf{D}^{r \times r}$ is a diagonal matrix, where the diagonal contains the $\sigma_i = \sqrt{\lambda_i}$ which are known as the singular values of \mathbf{X} and λ_i for $i = 1, 2, \dots, r$ are nonzero eigenvalues of $\mathbf{X}\mathbf{X}^T$. The decomposition can be rewritten as:

$$\mathbf{X} = \mathbf{U}_r \mathbf{D} \mathbf{V}_r^T = \sum_{i=1}^r \sigma_i \mathbf{u}_i \mathbf{v}_i^T$$

Thus, setting the eigenvalue problem as follows:

$$\begin{cases} \mathbf{X}\mathbf{X}^T \mathbf{u}_i = \lambda_i \mathbf{u}_i, i = 1, 2, \dots, r \\ \mathbf{X}^T \mathbf{X} \mathbf{v}_i = \lambda_i \mathbf{v}_i, i = 1, 2, \dots, r \end{cases}$$

The symmetric matrices $\mathbf{X}\mathbf{X}^T = \mathbf{X}^T \mathbf{X}$ (whether they are real or complex) share the same eigenvalues and the respective eigenvectors are *orthogonal*. By normalizing them to the unit norm they become *orthonormal*, meaning that $\mathbf{u}_i^T \mathbf{u}_i = 1$ and $\mathbf{v}_i^T \mathbf{v}_i = 1$.

$$\mathbf{u}_i = \frac{1}{\sigma_i} \mathbf{X} \mathbf{v}_i, i = 1, 2, \dots, r$$

Now, using that $\mathbf{u}_{i=1, \dots, r}, \mathbf{v}_{i=1, \dots, r}$ are the eigenvectors corresponding to non-zero eigenvalues and that $\mathbf{u}_{i=r+1, \dots, l}, \mathbf{v}_{i=r+1, \dots, l}$ correspond to zero eigenvalues, which means that $\mathbf{X} \mathbf{u}_{i=r+1, \dots, l} = \mathbf{0}$. Then for this latter case we can write that:

$$\sum_{i=1}^r \sigma_i \mathbf{u}_i \mathbf{v}_i^T = \mathbf{X} \sum_{i=1}^r \sigma_i \frac{1}{\sigma_i} \mathbf{v}_i \mathbf{v}_i^T = \mathbf{X} \sum_{i=1}^l \mathbf{v}_i \mathbf{v}_i^T = \mathbf{X} \mathbf{V} \mathbf{V}^T$$

Where \mathbf{V} is the unary matrix with columns the orthonormal eigenvectors \mathbf{v}_i , thus $\mathbf{V} \mathbf{V}^T = \mathbf{I}$, completing the claim of the decomposition.

2.3.1 Geometric interpretation

In the regression section we discussed the problem with ill-conditioned matrices and the use of the pseudo-inverse as a turnaround to this problem. Here we will make the connection of the pseudo-inverse to SVD, concluding with the geometric interpretation.

In linear regression the problem was to find the optimal vector \mathbf{w} given a set of observations:

$$\hat{\mathbf{w}} = \arg \min_{\mathbf{w}} \|\mathbf{y} - \mathbf{X}\mathbf{w}\| = \arg \min_{\mathbf{w}} \sum_{n=1}^N (y_n - \mathbf{w}^T x_n)^2 = \arg \min_{\mathbf{w}} \|\mathbf{e}\|^2$$

this task seeks the minimization of the error vector $\mathbf{e} = \mathbf{y} - \mathbf{w}^T x_n$.

where $\|\cdot\|$ is the Euclidean norm, functioning as a distance metric between the respective vectors in \mathbf{y} and $\mathbf{X}\mathbf{w}$ in R^n .

Let the columns of \mathbf{X} be defined as $\mathbf{X} = [\mathbf{x}_1, \dots, \mathbf{x}_l]$

$$\hat{\mathbf{y}} := \mathbf{X}\mathbf{w} = \sum_{i=1}^l \mathbf{w}_i \mathbf{x}_i$$

$$\mathbf{e} = \mathbf{y} - \hat{\mathbf{y}}$$

As a result $\hat{\mathbf{y}}$ represents a vector that lies in the $\text{span}(\mathbf{x}_1, \dots, \mathbf{x}_l)$. Thus, the minimization problem is precisely to find the \mathbf{w} for which the error between \mathbf{y} and $\hat{\mathbf{y}}$ has the *minimal norm*. Based on the Pythagorean theorem of orthogonality for Euclidean spaces this is achieved if $\hat{\mathbf{y}}$ is chosen as the orthogonal projection of \mathbf{y} onto the $\text{span}(\mathbf{x}_1, \dots, \mathbf{x}_l)$. The projection is illustrated in Figure 5.

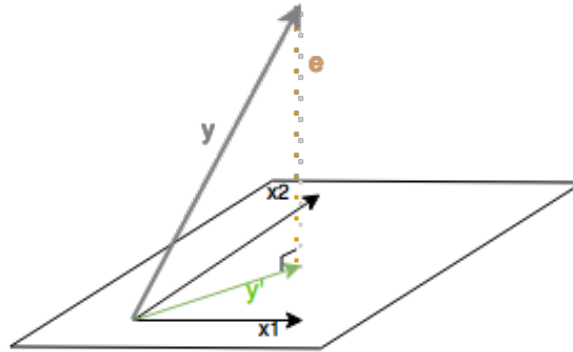


Figure 5: geometric interpretation of least squares for $l=2$

Based on the concept of orthogonal projections the *least squares estimate* is concluded as follows (using the dagger for the pseudo-inverse):

$$\hat{\mathbf{y}} = \mathbf{X}(\mathbf{X}^T \mathbf{X})^{-1} \mathbf{X}^T \mathbf{y} = \mathbf{X}^\dagger \mathbf{y}$$

2.4 Principal Component Analysis

In the section of regression we explained how a model is optimized based on the minimization of the quantified disagreement with the observations. A slightly different interpretation is that with regression we acquire a linear combination of independent variables that provide the best prediction based on the dependent variables. Keeping this, we can alter the definition of the linear combination in various ways to describe different learning problems. In *canonical correlation* for instance, the linear combination is defined based on a subset of variables, which have been chosen in a way that provide maximum correlation with another subset of variables. Hence, canonical correlation is used in practice to maximally correlate two different groups of variables. In *discriminant analysis* the linear combination is constructed to maximally separate groups of observations (as we saw in SVMs the optimized hyperplane is defined by a discriminant function). *Principal Component Analysis* (PCA) focuses on a single sample of observations, assuming their existence based on a hidden (latent) composition of some variables, to be learned.

The process for finding the assumed hidden structure, is done by specifying groups of linear combinations that express the maximal variance in descending order. These linear combinations are named *principal components*. The principal components are found through searching all the possible directions to which the observations become maximally spread out, then ordered in descending order depending on the explained variance. Thus, the first principal component corresponds to the linear combination with the maximal variance, the second to a linear combination orthogonal to the first one explaining maximum variance and so on and so forth. The principality relates to that exact property of maximum variance representation and at the same time preserving uncorrelated hidden variables.

The problem of finding the direction of maximum variation is connected to solving the *generalized eigenvalue problem*

$$\mathbf{A}\hat{\mathbf{u}} = \lambda\mathbf{B}\hat{\mathbf{u}}$$

The solutions to generalized eigenvalue problem correspond to finding the extremum points¹ of a special case of the *Rayleigh quotient*:

$$r = \frac{\mathbf{w}^T \mathbf{A} \mathbf{w}}{\mathbf{w}^T \mathbf{B} \mathbf{w}}$$

with matrices \mathbf{A}, \mathbf{B} being symmetric and \mathbf{B} positive definite.

PCA can be found in the literature being mentioned as Hotelling transform. Originally it was developed by Pearson (1901) and Hotelling (1936) [9]. PCA can be also found being mentioned as Karhunen-Loève Transform as well.

From a practical point of view, in the case that the independent variables is large compared to the number of observations, it might be useful to use PCA for dimensionality reduction in

¹namely the points of zero derivatives of the ratio of quadratic forms

order to reveal patterns from a multidimensional dataset. The reduction is done through projecting² the dataset in the subspace with maximum variation. This subspace is spanned by the k -first principal components, just described. Thus, PCA can be seen also as a generator of uncorrelated features.

Consequently, a classifier can be applied in the reduced dataset to classify the visualized patterns. It is interesting to note that *Cover's theorem* states that when working in higher dimensional spaces, the probability of a classification task being linearly separable increases with the dimensionality of the space. Hence, depending on the dataset it might be more useful to use a classifier directly, or in case of a *sparse* data set to reduce the dimensionality with the best possible *low rank approximation*.

Using the notation from the SVD section, a *k-rank matrix approximation* means to find the best approximation matrix $\hat{\mathbf{X}}$, with rank $k < r \leq \min(m, l)$ defined as follows:

$$\hat{\mathbf{X}} = \sum_{i=1}^k \sigma_i \mathbf{u}_i \mathbf{v}_i^T$$

counting the approximation error with:

$$\|\mathbf{X} - \hat{\mathbf{X}}\|_F = \sqrt{\sum_{i=k+1}^r \sigma_i^2}, \text{ in the case of } \textit{Frobenius} \text{ norm}$$

or

$$\|\mathbf{X} - \hat{\mathbf{X}}\|_2 = \sigma_{k+1}, \text{ in the case of } \textit{Spectral} \text{ norm}$$

An inspection of the eigenvalues should always take place to see if it is reasonable to lose a certain amount of information in order to see the patterns (choosing the first 2 or 3 principal components), or in general set a threshold from the point where the explanation in variance starts reducing dramatically. At certain applications, when the observable is a fluctuating vector, containing the information of a signal, the information loss is understood as a *denoising* effect or even *quantization* of the signal [1]. Due to the connection of PCA to the eigenvalue problem, which as presented in the previous section is also connected to SVD, SVD is also used as a reference to refer to applications of PCA.

In Chapter 4 the exact description of the chosen algorithm is provided for the implementation of the low-rank approximation as well as the approximation errors for a quantified realization of the approximation quality using the presented norms.

²the projection can be done also in feature space (kernel-PCA) [16]

3 The Large Hadron Collider

3.1 Overview

The Large Hadron Collider (LHC) consists of eight arcs and eight straight regions, built between the Swiss-French borders, at an average depth of 100 meters under the earth surface and with an operational³ circumference approximated at 26659 m.

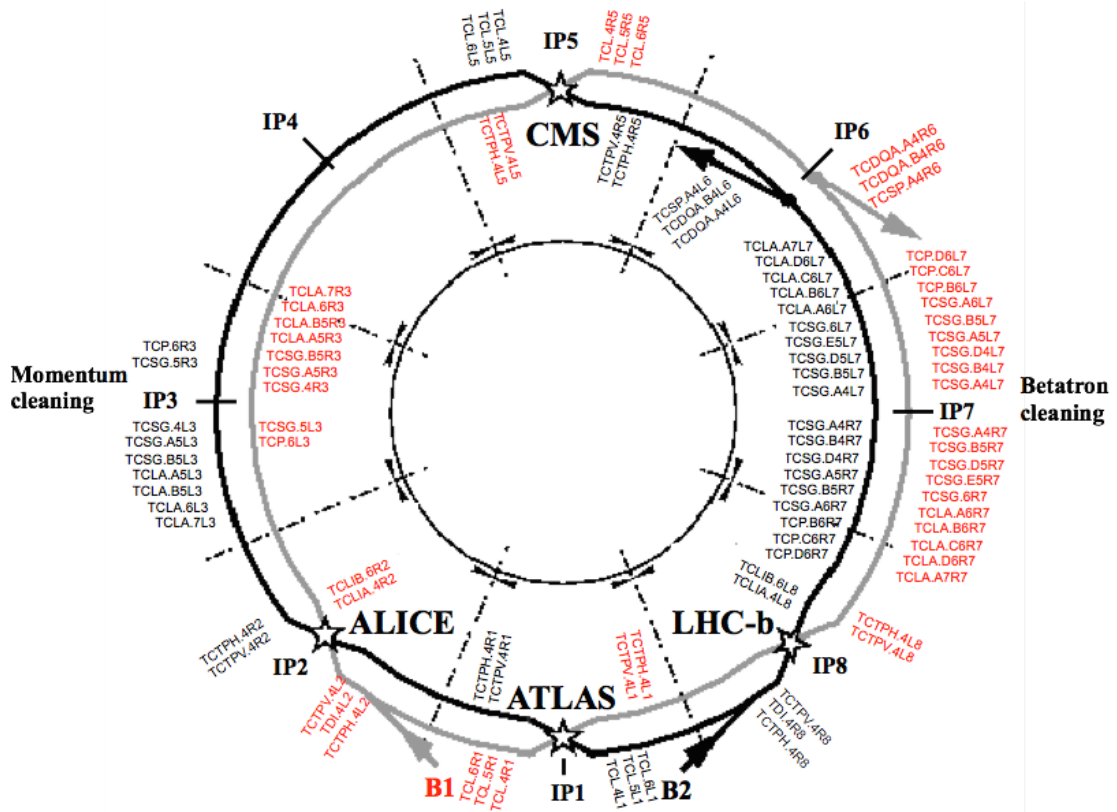


Figure 6: LHC map [14]

The LHC accelerates particles in two counter-rotating beams and a series of steps (injection, energy ramp, flat-top and squeeze) are performed prior to bringing the two beams in collision in the interaction points IP1, IP2, IP5 and IP8, where the experiments ATLAS, ALICE, CMS and LHCb are installed. The insertion region IR4 contains the Radio-Frequency system (RF) of LHC.

The specification of LHC is available in Table 1, with the corresponding parameters. These are the nominal parameters referring to the designed performance of LHC.

³the LHC shrinks approximately 80 meters when cooled down to almost absolute zero Kelvin

| Property | Nominal Value |
|----------------------------------|------------------------|
| Energy | 7 TeV |
| Number of proton bunches | 2808 |
| Protons per bunch | $1.15 \cdot 10^{11}$ p |
| Proton Beam Intensity | $3.2 \cdot 10^{14}$ p |
| Minimum bunch spacing | 25 ns |
| Revolution period | 88.924 μ s |
| Revolution frequency | 11 245 Hz |
| Collision rate | 600 MHz |
| Energy stored per colliding Beam | 362 MJ |

Table 1: LHC specification

3.2 Collimation system

3.2.1 Purpose

Unavoidable beam losses from the high-energy beams can result in quenches⁴ of the superconducting magnets or even damage of components. To protect the machine from such jeopardizing events a collimation system - grouped in multiple stages - is installed in LHC [4]. Most collimators in LHC are equipped with two movable jaws (see Figure 7). The purpose and challenge of the collimation system is to clean beam halo and offer protection against radiation effects [2].



Figure 7: an LHC collimator [14]

The two straight Insertion Regions of IR3 and IR7 contain the main part of the collimation system, designed to clean off-momentum particles and particles with high betatron amplitudes respectively. The design of the collimation system in IR3 and IR7 is based on the same design principle, consisting of primary collimators (TCPs), closest to the beam to intercept primary halo, then followed by the secondaries (TCSGs) for intercepting secondary halo. In the end of the hierarchy active absorbers (TCLAs) are placed, in order to absorb tertiary halo particles. The tertiary collimators (TCTs) are positioned before the experimental IPs to protect the experiments. Additional collimators are located in IP6 to protect the beam dump and at the two injection lines in IR2 and IR8.

Particles escaping the aforementioned cleaning hierarchy (Figure 8) deposit energy downstream of the betatron collimation insertion to the cold magnets in the dispersion suppressor (DS). In particular, the energy deposition in DS originates from single-diffractive interactions in the primary collimators [10]. During operation with heavy ions, fragmentation can cause similar limitations [3].

⁴quench is an event where a superconducting magnet returns to its resistive state, becoming normal conducting.

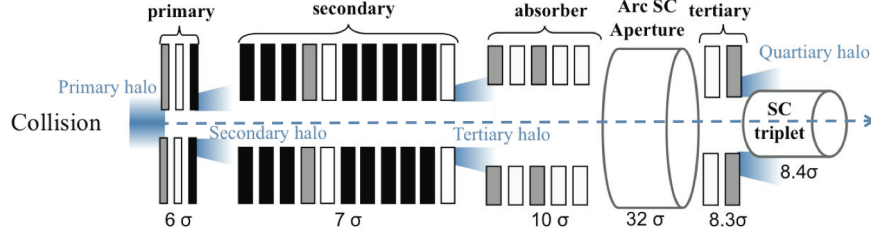


Figure 8: collimation hierarchy showing the nominal settings in units of beam sigma [14]

3.2.2 Jaw movement

Responsible for the jaw movement are the stepper motors, shown in Figure 9, which execute predefined trajectories, based on a kinematic chain, without relying directly on a feedback mechanism. In order to measure the jaw movement in real time, Linear Variable Differential Transformers (LVDTs) are used as displacement sensors.

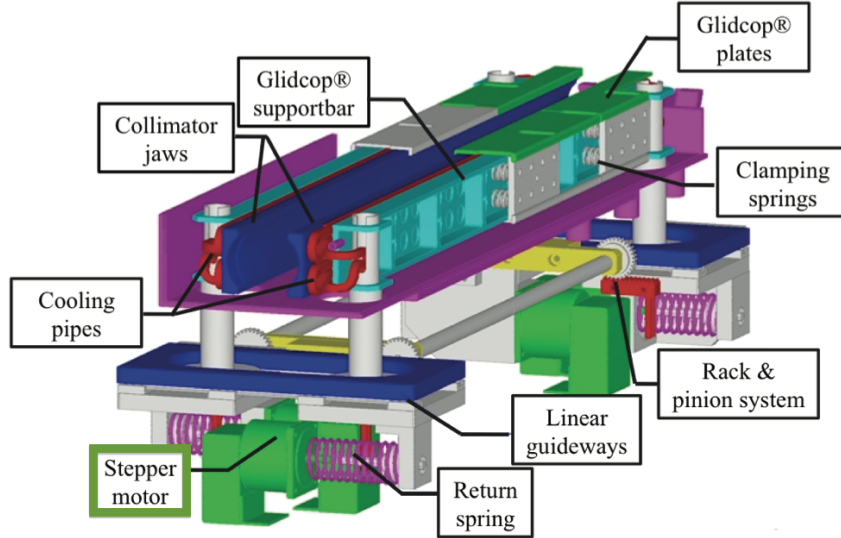


Figure 9: design of a collimator [14]

The working principle of the LVDT is fundamental and is used in the industry (e.g robotics, control, aerospace) since the 1930s. It consists of a primary winding excited by alternating signal and two secondary ones to which the signal is induced. The displacement $x_{[mm]}$ of the moving target between the primary and secondary windings can be estimated based on the output signals from the secondaries, defined by the amplitude A , frequency f and phase ϕ (see Figure 10).

Due to the very high radiation doses (MGrays/year) in the location of LHC collimators, the installation of electronics in this area for conditioning the output LVDT signal is not applicable. The electronics are placed several hundred meters or even kilometers away from the collimators, which create an additional matching problem for conditioning the output signal from the LVDT. For this reason various conditioning techniques have been proposed

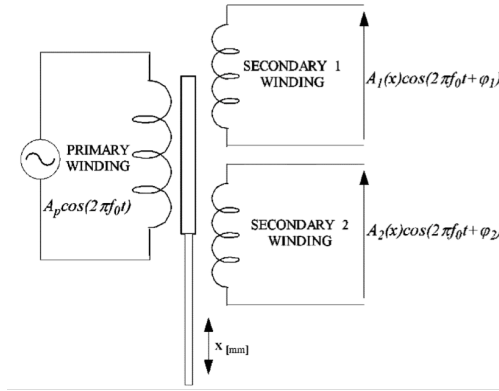


Figure 10: LVDT working principle [11]

in the literature. For the LHC collimators in particular [11] the sine-wave signal from the secondaries which arrives several hundreds of meters further to the electronics is reconstructed and then a ratiometric formula is used for the final displacement estimation. The reported LVDT accuracy in terms of 1σ is less than $1\mu\text{m}$. The recorded jaw positions can be retrieved from dedicated variables in the logging system, referring to the MOTOR configuration and the LVDT reading. More specifically for each jaw (left/right) the position of each edge is available (upstream/downstream). In the case of the LVDT reading the overall gap is also available (upstream/downstream). In the discussed settings later on, upstream and downstream configuration is assumed identical per collimator, namely non-tilted and non-deformed jaws.

3.2.3 Half gaps

The distance between the collimator jaw edge closest to the beam and the beam center can be used to calculate the *half-gap*, which is measured in sigmas, with respect to the distribution of the collimated beam at the measurement point.

The 1 sigma nominal beam size, assuming analysis of the beam distribution as a two dimensional gaussian, is calculated as follows for i_{th} collimator:

$$\sigma_i = \sqrt{(\beta_{x,i}\epsilon_{x,i} + (D_i\delta_p)^2) \cos^2(\psi_i) + \beta_{y,i}\epsilon_y \sin^2(\psi_i)}$$

Where β_i is the beta function at i_{th} collimator, ϵ_i the geometric beam emittance, D_i the dispersion, δ_p the r.m.s momentum spread of the particles and ψ_i the azimuthal angle of the collimation plane. The beam center at i_{th} collimator can be found as the midpoint between two correctly aligned jaws [19]. Another method for finding the beam center is by moving a scraper towards the core of the beam, till the beam is vanished.

The collimator settings in σ for the different collimator families are shown in Table 2.

| Coll. | IR | 2012-13 (4TeV) | Nominal (7TeV) |
|-------|-------|----------------|----------------|
| TCP | IR7 | 4.3 | 6.0 |
| TCSG | IR7 | 6.3 | 7.0 |
| TCLA | IR7 | 8.3 | 10.0 |
| TCT | IR1/5 | 9.0 | 8.3 |
| TCT | IR2/8 | 12.0 | 8.3 |

Table 2: collimator settings

3.3 Beam Loss Monitors

The unavoidable beam losses must be monitored. Hence, a set of approximately 5000 Beam Loss Monitors (BLMs) are installed in the LHC, where about 3600 of them are Ionization Chambers (ICs) [8].

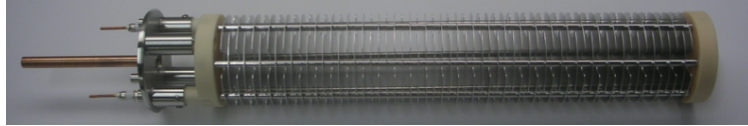


Figure 11: uncovered Ionization Chamber [14]

The *spatial distribution*⁵ of the losses in the tunnel, after deliberately blowing-up⁶ the beam, is known as a beam loss map. The visualization of the loss map demonstrates⁷ the beam losses (cleaning inefficiency) as a function of distance in the LHC tunnel. Contribution to the recorded losses is done as well due to additional ionization of the gas from cosmic rays, which empirically is said to correspond to approximately $3.5 \cdot 10^{-7}$ on a normalized logarithmic scale. The validation of a beam loss map is done by removing the noise after being measured experimentally, a step which we will call as *offset subtraction*.



Figure 12: Beam Loss Monitor attached on a focusing quadrupole [14]

The described process for performing a beam loss map is pursued after a beam based alignment (BBA) procedure [19], in order to validate the new operational collimator settings. A pre-processing step is also incorporated for subtracting the experimentally measured noise in the BLM signals, before the beam excitation is triggered. The recorded losses are then normalized downstream the primary collimators, where the maximum loss should appear. Two empty collimator slots coded as TCP.A6 are available for each betatron cleaning hierarchy (per beam) and thus the relevant attached BLM is used as a normalizer, for the respective excited beam.

The two beams in the LHC are studied independently. Nevertheless, *electromagnetic showers* are recorded in the opposite of the excited beam, a phenomenon which we will refer

⁵we will use this naming convention to refer to the location-wise occurrence of beam losses in LHC

⁶through the ADT transverse dumper or by crossing the third order tune resonance [13]

⁷a single BLM is represented by a vertical line, which length corresponds to the normalized magnitude of the BLM measurement and the line graphic effect the type of element of the accelerator, on which the BLM is attached on.

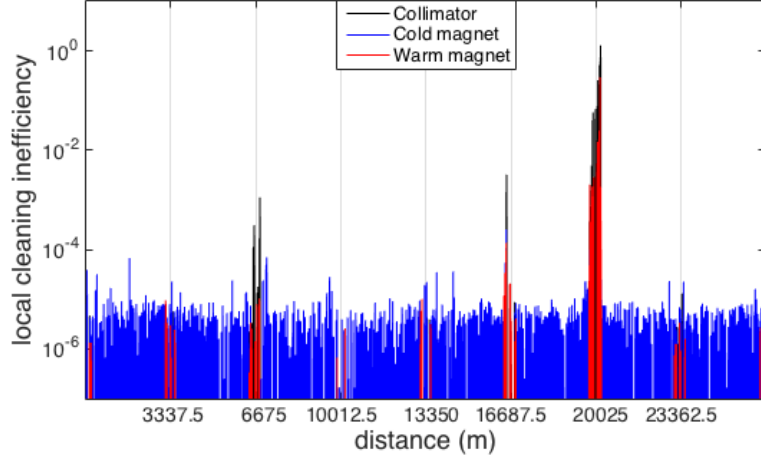


Figure 13: loss map on B2VER (IR 1-8)

to it as *crosstalk*. The principle when inspecting the collimation hierarchy is to verify the progressive reduction of the integrated beam losses from the primary collimators to the absorbers. Then the collimator settings are reviewed for further improvements. An additional inspection criterion is the beam losses recorded in the superconducting dipoles in the dispersion suppressor, downstream the collimation hierarchy. Particles scattered on primary collimators escape the straight cleaning hierarchy depositing their energy on the bending dipoles and thus DS in IR7 is considered the limiting location of LHC.

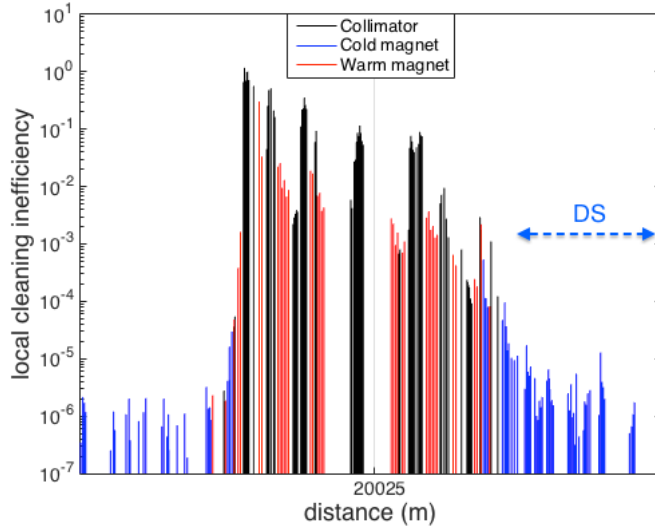


Figure 14: beam loss map on B1VER zoomed in IR7

The BLM names in the LHC are defined based on the naming convention attached below. In the next chapter we will refer to the BLM selection based on this naming convention.

Similarly, the collimator family acronyms are extended to provide further information for a collimator belonging to a given family. The extended collimator naming is as follows [14]:

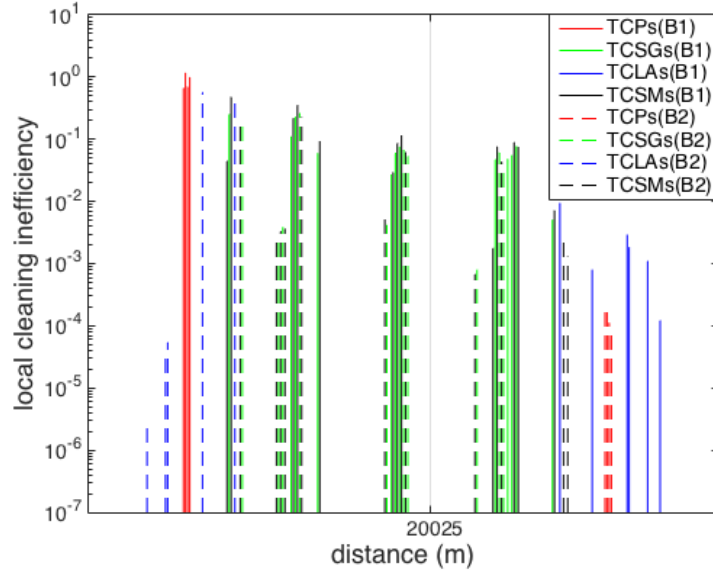


Figure 15: collimation loss map on B1VER - zoomed in IR7

| |
|---|
| BLM Q I . 06R7 . B1 E30 .MQMxxx(-S) |
| BLM = Beam Loss Monitor |
| Q = BLM location or feature (e.g T for Collimator E for Expert Q for Quadrupole) |
| I = Ionization Chamber type of detector |
| 06R7 = Position encoding |
| B1 = Beam one |
| E = Transverse Position |
| 30 = Position on the element |
| MQMxxx = observed element |
| S = additional information e.g Second coupled monitor |

Table 3: blm naming conventions

| | |
|---|---|
| TCP. D6 L7 . B1 (Layout) | TCP. IP7 . B1 . 1 . V (Display) |
| TCP - collimator family | TCP - collimator family |
| D6 - cell number | IP7 - 7th Interaction Point |
| L - Left of the IP | B1 - Beam one |
| 7 - IP | 1 - index in IR |
| B1 - Beam one | V - Vertical |

Table 4: collimator naming conventions

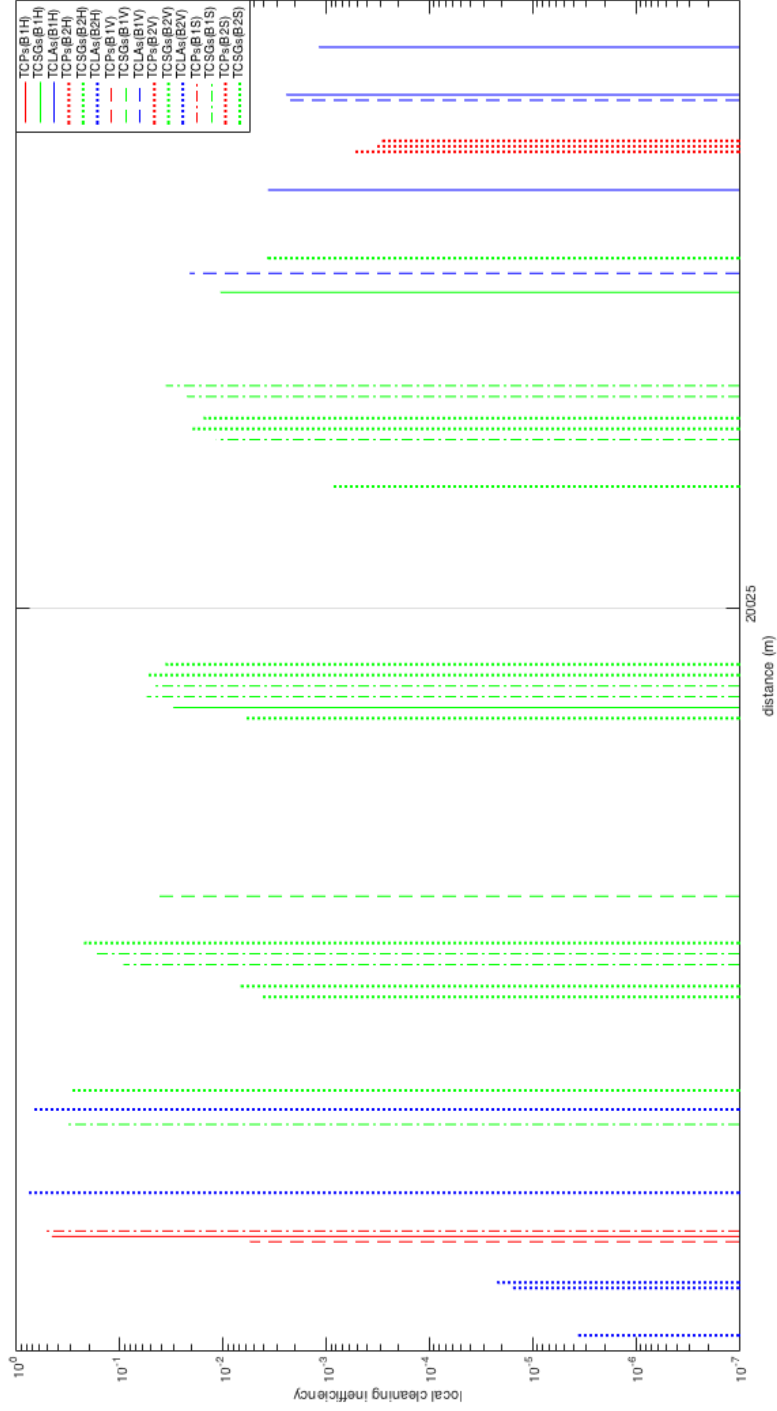


Figure 16: analytic collimation loss map on B1VER - zoomed in IR7

4 Learning from Beam Loss Monitors

In the two previous chapters we elaborated on the main methods arriving from the fields of statistical learning theory, multivariate analysis and described the main technical aspects of LHC, including the origin of the recorded data and how they are visualized to determine the performance of the LHC collimation system. In this chapter we present the application of such methods on the recorded datasets. Before concluding to the actual results, it is necessary to introduce the requirements that have been set in advance, that have tailored the data analysis steps and applicability of the methods accordingly.

4.1 Requirements

The visualization of the spatial distribution of beam losses across the whole LHC ring, as presented earlier, is done through the so-called beam loss maps. Due to the high number of ICs it is difficult to identify quickly abnormalities that might appear from loss map to loss map, especially when a group of timestamps is taken into account, that can be separated by weeks or even months of LHC operation. In this chapter we present an alternative approach for quantifying the loss map information by transforming the monitored losses in data points, embedded in n -dimensional spaces. The embedding of the beam loss information in such spaces, is necessary as the fluctuations in losses have to be expressed optimally through the position of the data point in this space.

Whilst each loss map is done for a selected beam and plane at a certain beam energy, in order to benchmark the corresponding collimation setup at that energy, the beam losses have been strictly separated in case studies (Beam/Plane/Energy) accordingly. Now, having selected a specific case study, our goal is to find patterns that are result of either major or minor abnormalities in the loss map hierarchy. Once the meaningful scenarios are identified, the use of a classifier takes place to classify the patterns as best as possible.

The loss maps under investigation concern the betatron cleaning hierarchy installed in IR7. Thus, the analysis is based on the monitors installed in that insertion, and in particular the ones attached on collimators (with certain exceptions as we will elaborate later). It is important to note in this point that the objective of this analysis is the spatial distribution of the beam losses in the betatron cleaning hierarchy.

The beam loss information is based on the accumulated beam losses recorded at certain integration time windows. The time length of the integration time window is controlled by the Running Sum (RS), the selected running sum for all case studies is the RS09, which corresponds to $2^{15} = 32768$ integration windows of $40\mu s$ totalling $1.31sec$.

4.2 BLM selection

In this section we commence with a detailed elaboration on the *data analysis* steps, providing logical and physical justifications on the exact BLM selection that was pursued having in mind the best possible representation of the spatial distribution of beam losses occurring at collimators.

This process involved several limitations, due to the fact that BLMs were updated, in their name and/or their location in the tunnel, making it non-trivial to directly retrieve a robust BLM group that remained intact, able to represent the same exact spatial distribution of losses, across all years of LHC operation. Before presenting the group of BLMs that remained (location-wise) intact between 2011-2015 we will discuss the technical aspects that concluded to the final selection.

In the current analysis we focus on Ionization Chambers (ICs). It is worth mentioning also that BLMs from both beams were kept for each betatron loss map (which is performed per beam and plane), due to the cross-talk effect described earlier, as well as BLMs attached on vertical, horizontal, skew collimators, as the excitation wave in one plane is translated also as excitation to the other plane, due to the coupled betatron motion of the beam.

These tables are updated each time the BLM setup was altered at the processed loss maps, listed from Table 23 to Table 26. After presenting in chronological order the BLM setup updates in IR7 collimator slots (including their longitudinal coordinate in the LHC tunnel), we conclude with a BLM subgroup which is compatible with all BLMs setups, allowing us to use this group for all processed loss maps between 2011 and 2015, retrieving the same spatial beam loss distribution for later comparisons. This subgroup is available in Table 27.

Prior to a loss map captured on 15-05-2011, two extra BLMs had been already attached on TCSG.A6R7.B2 and TCHSS.6R7.B2 collimators, resulting to 76 BLMs in total at IR7 collimators. From a loss map captured in 2012 one extra was attached at an empty slot indicated as TCSM.C5R7.B1 (77 BLMs in total). In 2015 the total number of BLMs at collimators increased to 84 and at the same time the first BLM substring was updated from BLMEI to BLMTI.

Thus, in order to be able to compare optimally the loss map hierarchies, a combination of name and location based selection of BLMs has been made, in order to ensure that the spatial distribution of losses under comparison, remains the same across all years of operation (rather than filtering BLMs solely by name). The name-location based selection retrieved several exceptional cases that have been recorded and are listed here:

One case was that some BLMs were installed on the same exact location. This case, in the processed timestamps, was result of two scenarios:

- Two BLMs installed at two neighboring TCSMs per beam. These two BLMs were present in all processed timestamps and were kept, as they did not occur incompatibilities among the processed timestamps.
- Two different types of BLMs on the same beam (ICs and LICs). In this case the Ionization Chambers were kept, due to the fact that LICs were designed with reduced volumes in order

to capture fast beam losses. Then when keeping the same integration time window with the ICs, the beam losses were physically incomparable.

The resulted selection of BLMs based on the above is attached in Table 27, consisting of 73 BLMs. The BLM naming used in 2015 was kept for the purposes of the table. This selection allows us to work on beam loss monitored data having as reference a *deterministic* physical system and consequently a controlled capacity for the learning problem later.

4.3 Data organization

The identification of beam loss pattern requires at first a dedicated collection of the data sets and organization of them in case studies with valuable physical meaning. The LHC beams are treated independently and the beam loss maps are performed for a pre-selected beam plane. The beam energy is also taken into account, avoiding mixing loss maps at different energies in the same data set. Thus, each loss map tuple is appended to the corresponding data set, which is defined based on a specific beam type, plane and beam energy.

Based on the elaborated requirements, a subset of BLMs, in total 73 (Table 27), will form the base for creating the data sets, on which we will refer to, in the next sections. The formal definition is as follows:

$$\mathbf{X} = [\mathbf{x}_1, \mathbf{x}_2, \dots, \mathbf{x}_{events}]^T$$

where an observable vector refers to spatial distribution of beam losses occurring at an approximate distance of 500 meters in IR7 of LHC, which is captured from the 73 BLMs discussed earlier. Thus, the input vector is defined as follows:

$$\mathbf{x}_t = [x_t^{BLM_1}, x_t^{BLM_2}, x_t^{BLM_3}, \dots, x_t^{BLM_{73}}]$$

With time t referring at the time of the loss map event, encoded by the UTC timestamp. We have already emphasized the importance of distinguishing loss maps based on the following criteria:

- Beam Type (Beam 1 or Beam 2)
- Beam Plane (Horizontal or Vertical)
- Beam Energy (450, 3500, 4000 GeV)

Thus, a data set of loss maps refers to a specific instance of the above cases. To state an example, the data set containing all beam loss maps performed on the horizontal plane of beam one at injection (450GeV) will be briefly named as B1HOR450 or else $\mathbf{X}_{B1HOR450}$ with Figure 17 completing the data set description:

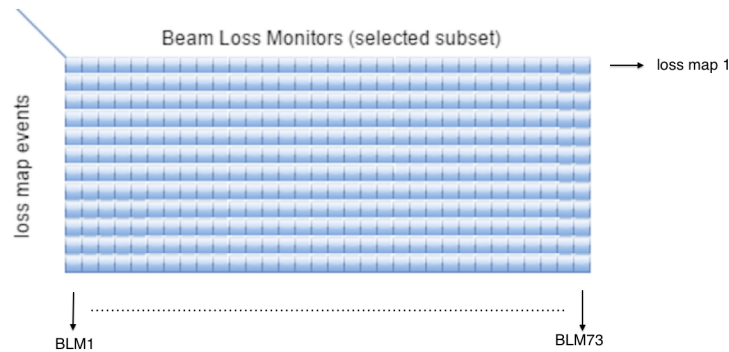


Figure 17: example of an extracted dataset for one case study (Beam/Plane/Energy)

4.4 Feature extraction

Based on the decided organization of the input datasets per case study (Beam/Plane/Energy), various ways of handling the 73 BLMs measurements have been researched.

Since the scope of the analysis is the interpretation of beam losses for collimation purposes (e.g automatic feedback for inspection of collimator settings), a detailed study was made to aggregate BLMs based on the collimator family that they are attached on. Initial experimentations of this decision retrieved preliminary results, though this solution derived concerns on the reliability of the averaged BLMs, due to the fact that a single BLM recording several orders of magnitude higher losses could be masked from the values of other BLMs. Taking also into account implications when neglecting local high beam losses (based on energy deposition studies e.g impact limits and deformation of jaws from heat load) this feature generation method was bypassed.

In the implemented and presented approach we consider feature extraction based on the principal component analysis method. As presented in the respective section, our task is to learn the hidden structure of a given dataset. This step relies only on the input dataset and thus being applied as an *unsupervised* feature extraction method, with no use of any prior information⁸. The input data set is based on a physical selection of Beam Loss Monitors, which was discussed earlier.

The transformation of the input data set to the lower dimensional, is done as follows for $k = 2$:

$$\hat{\mathbf{X}}^{events \times 2} = \mathbf{X}^{events \times 73} \cdot \hat{\phi}(\mathbf{u})^{73 \times 2}$$

Where $\hat{\phi}(\mathbf{u})$ is the feature map constructed by solving the eigenvalue problem presented in the second chapter and selecting the first two eigenvectors (corresponding to the first two eigenvalues in descending order). Thus the feature vector is two dimensional and the tuples of the transformed data set correspond to instances of the two dimensional feature vector, or else formally defined:

$$\mathbf{x}_f = [x_{\lambda 1}, x_{\lambda 2}] \text{ with } \hat{\mathbf{X}} = [\mathbf{x}_{f1}, \dots, \mathbf{x}_{f_{events}}]^T$$

Since the defined case studies are treated independently, the feature scaling process takes place for the features involved in each case study. This will be evident from the scaled axes that we will present later, as they will differ from case to case. The scaling takes place prior to splitting the dataset to training and testing samples, in order to ensure that the ones consisting of large numeric values, will not dominate the remaining ones and that the model will be defined on the scaled space during the training process.

When a collimation alignment is established the beam orbit drifts over time, and thus the recorded beam loss patterns deviate accordingly. For this physical reason, prior to reducing

⁸application of *supervised* dimensionality reduction is also possible, where a separate transformation is created for each class.

the dimensionality of the dataset, a random permutation is applied to the tuples of the data set \mathbf{X} , as they are ordered in chronological order during the data acquisition.

Hence, $\hat{\mathbf{X}}$ contains the extracted features from the original dataset, which are then scaled as follows per case study (Beam/Plane/Energy):

$$\frac{x - x_{min}}{x_{max} - x_{min}}$$

The feature scaled, randomly permuted, transformed data set is then used for the application of statistical learning (Figure 30).

The eigenvalues retrieved have been plotted per case study (Beam/Plane/Energy) and sorted in descending order. The visualization of the ordered eigenvalues provides insight of the dominating eigenvalues that explain variance in the data set, as for example at 450 GeV in Figure 19.

All discussed scenarios are based on the selection of the first 2 eigenvalues, which in total explain more than 90% of the dataset. The remaining percentage is considered as information lost when transforming the input data set to the projected data set in two dimensional space. This can be visualized in Figure 18, where the data points defined in 2D points are projected to the vector explaining maximum variance reducing them to one dimension. The information loss occurs when different data points are projected in the same coordinate of the lower dimensional space (Figure 18).

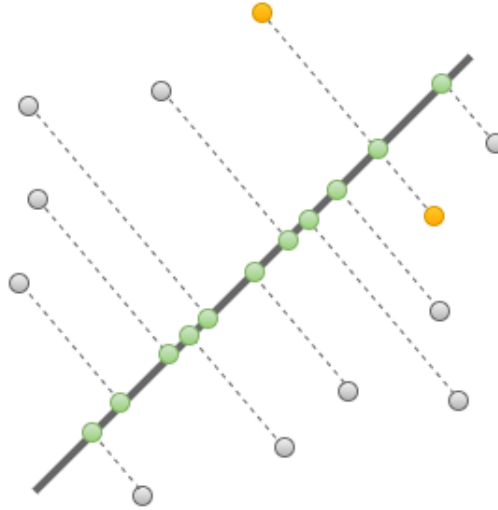


Figure 18: orthogonal projections

| Case Studies | 1st eigenvalue | 2nd eigenvalue | Total |
|--------------|----------------|----------------|--------|
| B1HOR450 | 86.33% | 11.81% | 98.14% |
| B1VER450 | 75.76% | 22.45% | 98.21% |
| B2HOR450 | 82.13% | 12.99% | 95.12% |
| B2VER450 | 91.80% | 5.50% | 97.30% |
| B1HOR3500 | 98.95% | 1.03% | 99.98% |
| B1VER3500 | 92.80% | 7.00% | 99.80% |
| B2HOR3500 | 99.95% | 0.04% | 99.99% |
| B2VER3500 | 98.04% | 1.93% | 99.97% |
| B1HOR4000 | 84.05% | 15.75% | 99.80% |
| B1VER4000 | 92.35% | 7.47% | 99.82% |
| B2HOR4000 | 98.78% | 0.91% | 99.69% |
| B2VER4000 | 94.89% | 5.07% | 99.96% |

Table 5: eigenvalue percentages

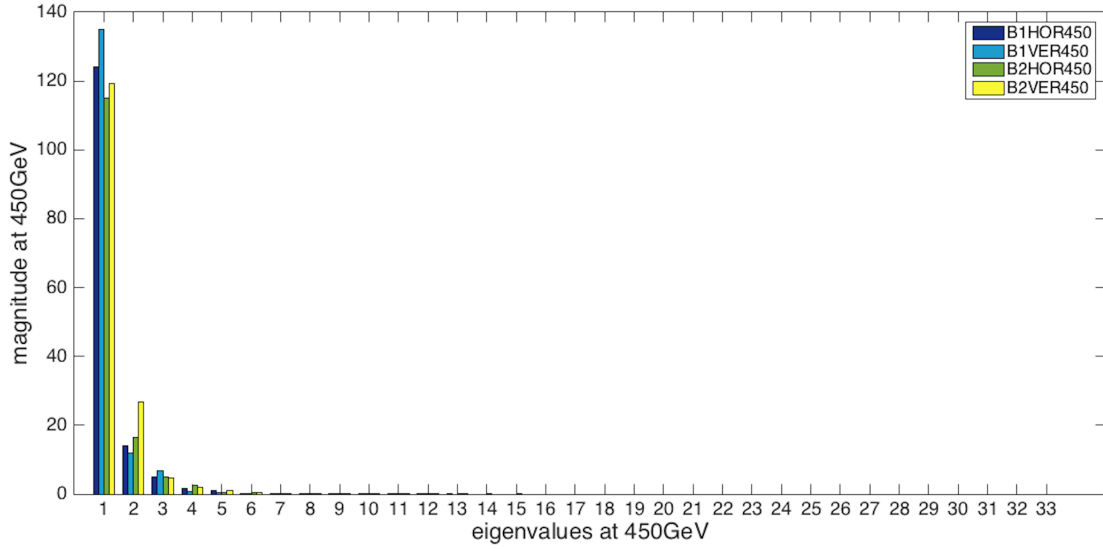


Figure 19: eigenvalue decay at 450 GeV

For brevity the percentages corresponding to the first two eigenvalues will be reported numerically in Table 5, without repeating the eigenvalue decay figures.

Motivated by the robust explanation of variance based on the first two eigenvalues and for the practical purposes of this thesis, the selected rank for the approximation selected is $k = 2$, allowing us to visualize the beam loss maps in 2D space as data points (or patterns). In the next chapter we will focus on very specific scenarios, choosing the respective data set of a case study and inspecting the collimator settings, in order to discover the effect of setting changes on the 2D patterns.

4.5 Identification of beam loss patterns

4.5.1 Major collimator setting changes

In this case study we analyze setting changes at a TCLA and the resulted hierarchy breakdown in the collimation hierarchy, elaborating on how the beam loss hierarchy can become broken when the half gap at a collimator reduces significantly in terms of beam sigma. Hence, the motivation of beam loss maps is built reversely, by inspecting them optimally, to find setting changes at individual collimators, which diverge from the standard collimator settings. This justifies the importance of identifying abnormal beam loss patterns, with the introduction of additional methods to aid this purpose. The section starts with a detailed elaboration of how a collimator setting analysis is pursued and concludes with the demonstration of the beam loss patterns as data points in 2D space.

During an alignment campaign at flat top in 2013, the TCLA.A6L7.R2 was misaligned by approximately $685\mu\text{m}$. A loss map focused in IR7 at incorrect settings is shown in Figure 20, demonstrating as well the effect of broken hierarchy to the recorded losses in the cold magnets in the Dispersion Suppressor (DS). For comparison of a normal loss map on the same beam/plane/energy is provided in Figure 21. The presented losses have been normalized with respect to the recorded losses at a reference BLM placed in an empty collimator slot (TCP.A6), downstream the IR7 primary collimators. Furthermore, the beam losses in the cold magnet Q8, often used for benchmarking of cleaning inefficiency [15], are shown in Table 6 for each associated BLM. With the shifted settings, the DS losses are about a factor of 1 higher.

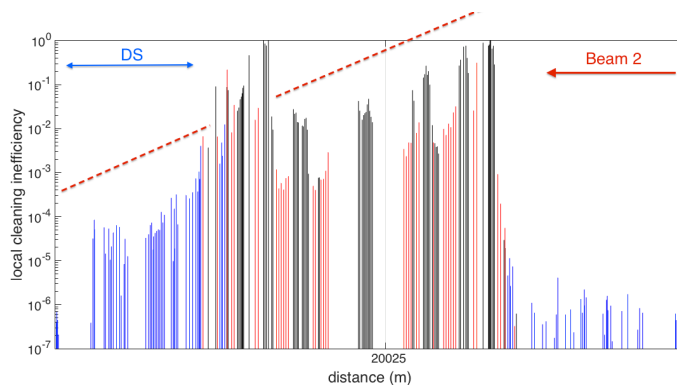


Figure 20: broken hierarchy on B2VER loss map at 4000 GeV

The incorrect settings resulted in a major shift of the collimator jaw center, forcing the TCLA.A6L7.B2 to be almost at the level of a primary collimator. An attempt was made to calculate the new half-gap in units sigma, by considering as correct center the one at the second timestamp. When a one sided cut is made, as in our case study, the beam distribution will be eventually redistributed to a Gaussian one (see Figure 22), allowing us to formulate it parametrically [5]. The estimated operational cut was due to the left jaw, which shifted closer to the correct beam center. Tables 7 and 8 summarize the upstream and downstream collimator settings respectively. We assumed also zero dispersion. The nominal

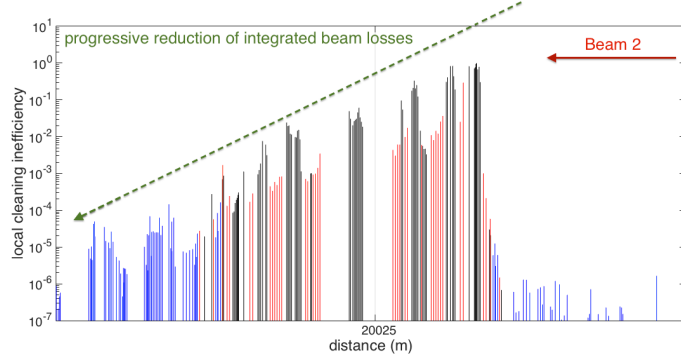


Figure 21: normal hierarchy on B2VER loss map at 4000 GeV

beam parameters in the referred timestamps were $\beta_y = 48.15m$ and geometric emittance $\epsilon = 8.21 * 10^{-10}m$.

| | | |
|---------------------|---------------------|---------------------|
| BLMQI.08L7 | 17/01/2013 16:47:22 | 02/02/2013 06:58:06 |
| B2I30_MQ (exit) | 2.9544e-04 | 6.6282e-05 |
| B2I20_MQ (middle) | 1.8318e-04 | 2.2132e-05 |
| B2I10_MQ (entrance) | 3.5015e-04 | 1.5585e-05 |

Table 6: beam losses in magnet Q8 in DS

| | | |
|--------------------------|-------------------------------|-----------------------------|
| TCLA.A6.L7.B2 (upstream) | 17/01/2013 16:47:22 | 02/02/2013 06:58:06 |
| LU (MOTOR/LVDT) | 1.3050/1.3082 (mm) | 1.9900/2.0065 (mm) |
| RU (MOTOR/LVDT) | -1.9950/-1.9949 (mm) | -1.3150/-1.3232 (mm) |
| CU (MOTOR/LVDT) | -0.69/0.6867 (mm) | -0.065/0.6833 (mm) |
| Half Gap (MOTOR/LVDT) | 4.86/4.76 σ (abnormal) | 8.30/8.37 σ (normal) |

Table 7: TCLA.A6L7.B2 alignment for broken and normal hierarchy (upstream)

| | | |
|----------------------------|-------------------------------|-----------------------------|
| TCLA.A6.L7.B2 (downstream) | 17/01/2013 16:47:22 | 02/02/2013 06:58:06 |
| LD (MOTOR/LVDT) | 1.3050/1.2886 (mm) | 1.9900/1.9884 (mm) |
| RD (MOTOR/LVDT) | -1.9950/-1.9933 (mm) | -1.3150/-1.3269 (mm) |
| CD (MOTOR/LVDT) | -0.69/-0.7047 (mm) | 0.675/0.6615 (mm) |
| Half Gap (MOTOR/LVDT) | 4.86/4.81 σ (abnormal) | 8.30/8.33 σ (normal) |

Table 8: TCLA.A6L7.B2 alignment for broken and normal hierarchy (downstream)

Tables 7 and 8 show that the estimation of the half-gap in sigma relies heavily on the sensor measurement taken into account and thus the importance to verify all sensors when inspecting the settings at a collimator. This motivates the goal of finding settings imperfections based entirely on beam loss maps, reversing the process from inspecting collimator settings, to inspecting beam loss maps, which in this thesis are enhanced further. For instance, the mapping in two dimensional space is illustrated in Figure 22, with point 17 indicating the loss map with the TCLA misalignment. A complete table of the correspondences of the enumerations to UTC timestamps is provided in Table 9.

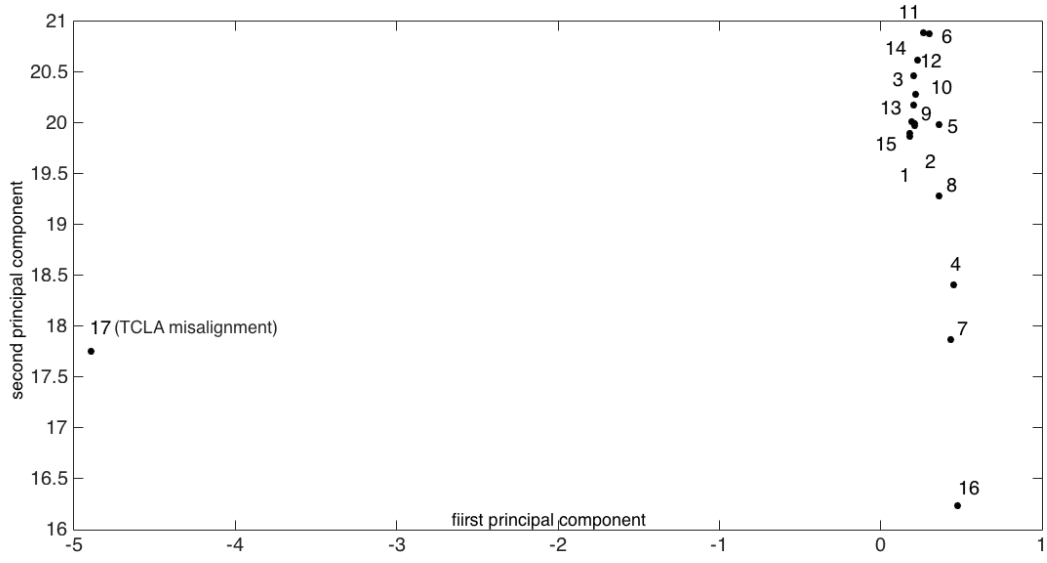


Figure 22: beam loss map B2VER patterns at 4000GeV.png

| Event | UTC | Date (GMT+2:00) |
|---------------|------------|----------------------|
| 1 | 1333025966 | 29 Mar 2012 14:59:26 |
| 2 | 1333026099 | 29 Mar 2012 13:01:39 |
| 3 | 1333148173 | 30 Mar 2012 22:56:13 |
| 4 | 1333382588 | 02 Apr 2012 18:03:08 |
| 5 | 1333382647 | 02 Apr 2012 16:04:07 |
| 6 | 1333383209 | 02 Apr 2012 16:13:29 |
| 7 | 1333420107 | 03 Apr 2012 04:28:27 |
| 8 | 1333420323 | 03 Apr 2012 04:32:03 |
| 9 | 1335777444 | 30 Apr 2012 11:17:24 |
| 10 | 1335822713 | 30 Apr 2012 23:51:53 |
| 11 | 1341114479 | 01 Jul 2012 05:47:59 |
| 12 | 1341158237 | 01 Jul 2012 17:57:17 |
| 13 | 1348632621 | 26 Sep 2012 06:10:21 |
| 14 | 1355250927 | 11 Dec 2012 19:35:27 |
| 15 | 1355257777 | 11 Dec 2012 21:29:37 |
| 16 | 1355272133 | 12 Dec 2012 01:28:53 |
| 17 (abnormal) | 1358437642 | 17 Jan 2013 16:47:22 |

Table 9: B2VER4000

4.5.2 Minor collimator setting changes

In the previous case study we investigated in detail the impact of a major setting change at a single collimator and the resulted footprint in the 2D space, reflecting correctly the abnormal pattern. In this case study we discuss setting changes at the level of $200\text{ }\mu\text{m}$, to observe the BLM sensitivity response in traditional beam loss maps and their resulted footprint in 2D space.

A dedicated session was planned during LHC Run II in 2015 at the Cern Control Center (CCC) to apply shifts in the jaw midpoints of pre-chosen collimators and collect the respective measurements for the scope of the pattern identification analysis. All tests were performed with LHC configured at injection beam mode⁹ (450GeV). Table 10 summarizes the collimators in which the jaw-shifts have been applied, covering all Beam/Plane case studies at injection energy, which will be reported in this section. When switching the collimator settings the settings of the previously adjusted collimator were reverted to the initial ones. Table 11 summarizes all loss map events per case study in chronological order, including the ID correspondences assigned to the 2D patterns presented in Figures 23, 24, 25 and 26.

An additional requirement introduced in the current analysis is that in parallel to the collimation tests, BLM tests were reported being performed as well. This resulted to an artificial numerical addition to the BLM readings. Since the scope of the collimation test was to observe the sensitivity of BLMs under collimation setting changes, the artificial offset was measured carefully in order to remove it and derive the true BLM readout. For this the offset subtraction technique reported earlier was included during the pre-processing process, by choosing a time window where no ADT blow-up occurred.

| Timestamp | Time | Case study | Collimator | Midpoint shift |
|------------|----------|------------|-----------------|--------------------------|
| 1432492325 | 20:32:05 | B1HOR450 | TCSG.IP7.B1.5.H | $200\text{ }\mu\text{m}$ |
| 1432492521 | 20:35:21 | B1VER450 | TCLA.IP7.B2.1.V | $200\text{ }\mu\text{m}$ |
| 1432492612 | 20:36:52 | B2HOR450 | TCLA.IP7.B2.4.H | $200\text{ }\mu\text{m}$ |
| 1432492750 | 20:39:10 | B2VER450 | TCSG.IP7.B2.4.V | $200\text{ }\mu\text{m}$ |

Table 10: jaw midpoint shifts (2015 test)

⁹an operational list of procedures named *sequence* is loaded.

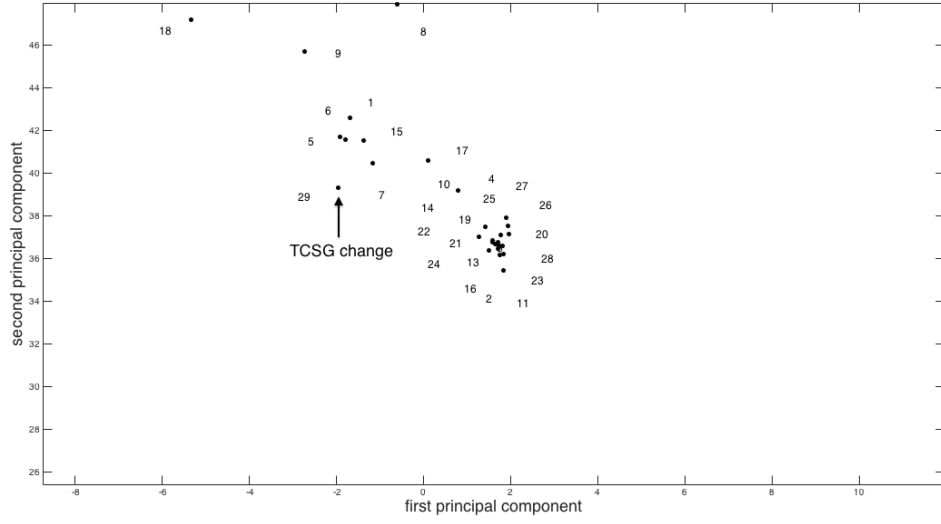


Figure 23: beam loss patterns for B1HOR Injection events

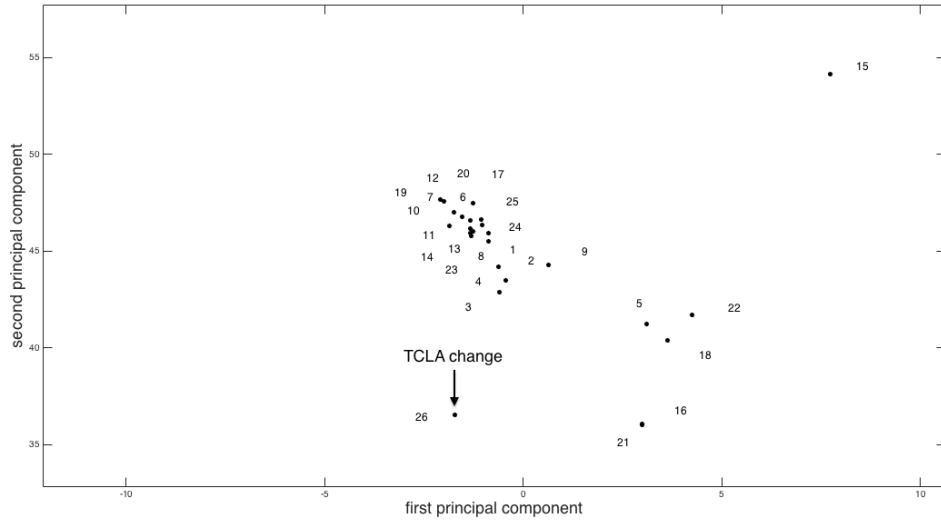


Figure 24: beam loss patterns for B1VER Injection events.png

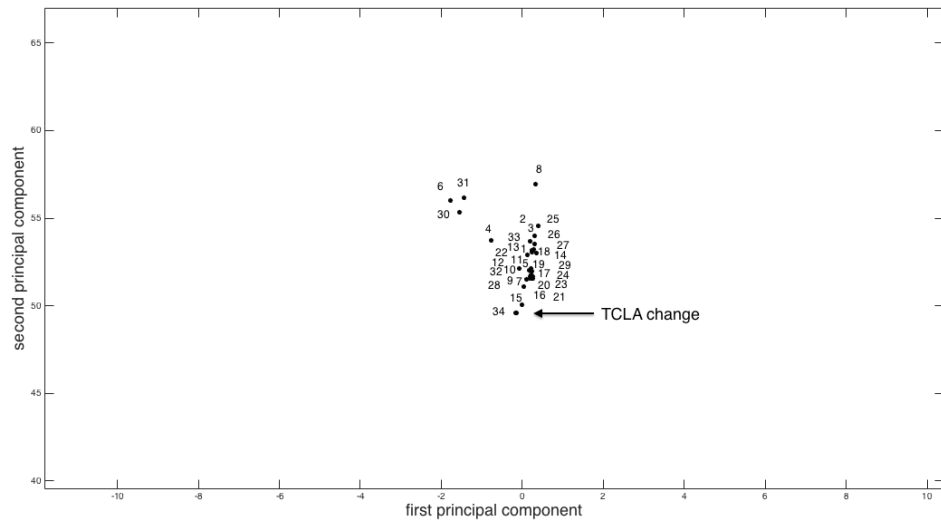


Figure 25: beam loss patterns for B2HOR Injection events.png

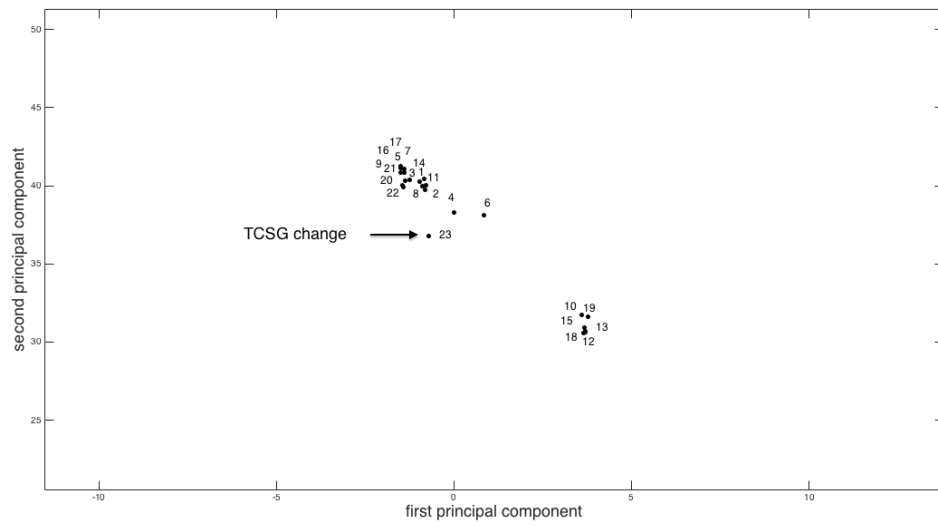


Figure 26: beam loss patterns for B2VER Injection events.png

| ID | B1HOR450 | B1VER450 | B2HOR450 | B2VER450 |
|----|-------------------|-------------------|-------------------|-------------------|
| 1 | 1299468812 | 1299466191 | 1299467039 | 1299466800 |
| 2 | 1299473383 | 1299472514 | 1299472719 | 1299472639 |
| 3 | 1299897855 | 1299897004 | 1299897906 | 1299897108 |
| 4 | 1301011709 | 1301011275 | 1301011804 | 1301011376 |
| 5 | 1301741427 | 1301011445 | 1301742030 | 1301741865 |
| 6 | 1301745684 | 1301741205 | 1301837533 | 1301837403 |
| 7 | 1301811446 | 1301745584 | 1301968659 | 1301968593 |
| 8 | 1301837134 | 1301811276 | 1301970912 | 1303644551 |
| 9 | 1301968427 | 1301836892 | 1303644789 | 1305586851 |
| 10 | 1301970629 | 1301968302 | 1303647849 | 1306253380 |
| 11 | 1303647811 | 1303647559 | 1305585822 | 1306491148 |
| 12 | 1304824398 | 1305757572 | 1306491281 | 1310612832 |
| 13 | 1305585680 | 1306252042 | 1310612733 | 1310615332 |
| 14 | 1306252381 | 1306491441 | 1310615263 | 1313016964 |
| 15 | 1306491548 | 1310612607 | 1312924236 | 1315262380 |
| 16 | 1310612462 | 1310615184 | 1313015231 | 1315295203 |
| 17 | 1310615111 | 1313016810 | 1314333908 | 1315296046 |
| 18 | 1312923280 | 1315261950 | 1314334560 | 1318919677 |
| 19 | 1313014588 | 1315294644 | 1314335568 | 1332611373 |
| 20 | 1315261723 | 1315295907 | 1314335850 | 1332614626 |
| 21 | 1315292164 | 1318918096 | 1314336585 | 1341170854 |
| 22 | 1318918021 | 1332611088 | 1315262179 | 1341171453 |
| 23 | 1332371851 | 1332614220 | 1315292514 | 1432492750 (2015) |
| 24 | 1332610921 | 1341170611 | 1318919568 | |
| 25 | 1332614082 | 1341171316 | 1332371667 | |
| 26 | 1333435914 | 1432492521 (2015) | 1332611287 | |
| 27 | 1341170425 | | 1332614447 | |
| 28 | 1341171231 | | 1341170736 | |
| 29 | 1432492325 (2015) | | 1341171393 | |
| 30 | | | 1358680228 | |
| 31 | | | 1358680916 | |
| 32 | | | 1360522198 | |
| 33 | | | 1360561128 | |
| 34 | | | 1432492612 (2015) | |

Table 11: UTC timestamps for proton beam loss maps at 450 GeV

4.5.3 Proton - Ion beams

LHC performs runs with ions at certain time periods. The losses recorded from BLMs at ion runs differ from the ones recorded at protons. The principle of collimation hierarchy has to be respected at both cases. In the context of investigating the spatial distribution of losses in LHC ring, a comparison of ion and proton loss maps was pursued using the aforementioned transformation, in order to observe the footprint of different particles interacting with collimators in 2D space. In particular, the time period related to the ions runs was in February 2013, where one beam pipe was filled with proton bunches and the other beam consisted of ion bunches, for collisions at ALICE experiment.

The beam loss patterns for the two different beam types are evident in Figures 27 and 28, with the ID correspondences made available in Table 12.

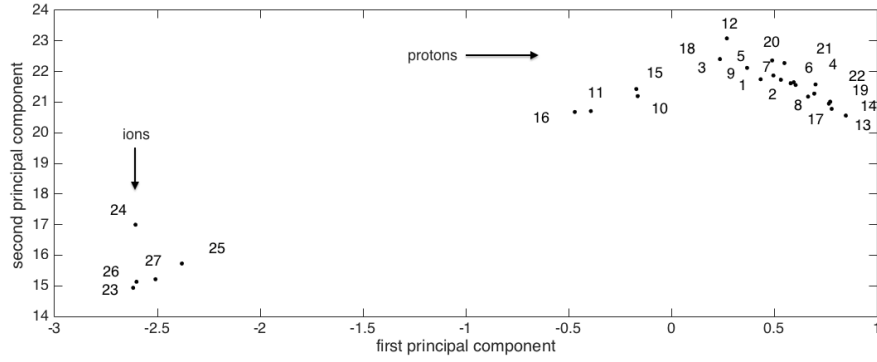


Figure 27: B1HOR proton-ion loss patterns

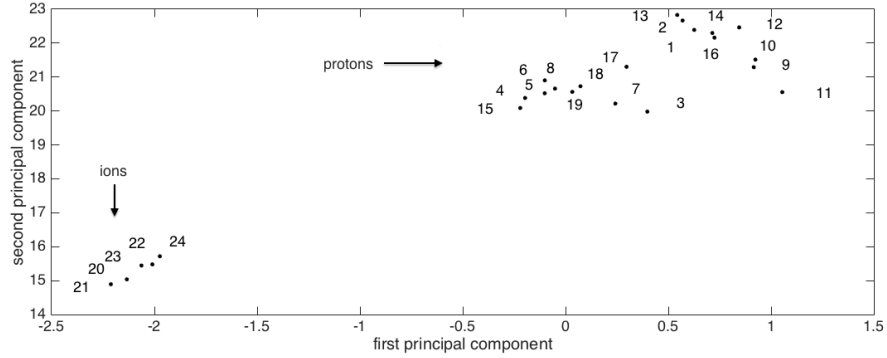


Figure 28: B1VER proton-ion loss patterns

| Event | UTC (B1HOR) | UTC (B1VER) |
|-------|-------------|-------------|
| 1 | 1333024960 | 1333025327 |
| 2 | 1333025088 | 1333025488 |
| 3 | 1333147902 | 1333148074 |
| 4 | 1333383458 | 1333383367 |
| 5 | 1333401421 | 1333419602 |
| 6 | 1333401465 | 1333419844 |
| 7 | 1333401509 | 1335777858 |
| 8 | 1333401609 | 1335822034 |
| 9 | 1335778233 | 1341113828 |
| 10 | 1335822397 | 1341158683 |
| 11 | 1341114091 | 1348632515 |
| 12 | 1341158426 | 1355217311 |
| 13 | 1348567464 | 1355250583 |
| 14 | 1355250439 | 1355256279 |
| 15 | 1355255874 | 1355271780 |
| 16 | 1355271558 | 1358530672 |
| 17 | 1358530410 | 1358543019 |
| 18 | 1358539961 | 1358619105 |
| 19 | 1358553743 | 1359336370 |
| 20 | 1358618928 | 1359751081 |
| 21 | 1358698268 | 1359784237 |
| 22 | 1359336152 | 1359792557 |
| 23 | 1359750736 | 1359794046 |
| 24 | 1359784055 | 1359806332 |
| 25 | 1359792488 | |
| 26 | 1359793963 | |
| 27 | 1359806207 | |

Table 12: proton - ion B1 loss maps combined

4.6 Classification of beam loss patterns

In the previous section the objective was the inspection of loss maps and identification of beam loss patterns, in order to verify the correctness of the physical pre-processing steps, as well as the projection of the BLM measurements into a lower dimensional space. In this section we build on this by classifying the identified patterns, introducing at the same time additional case studies. Once classified we focus on the data points being most dissimilar to the overall trend, and track back by inspecting the original beam loss map.

We look at proton runs, between 2011 - 2013 plus 2015. Any timestamp corresponding to an ion beam loss map has been filtered. Furthermore, special cases with beam loss monitors switched off or facing a temporary problem have been identified and the corresponding loss maps have been filtered. Loss maps with not sufficient beam intensity have been removed as well as they did not provide clear resolution of the beam loss spatial distribution in the LHC ring.

The classification is done through the elaborated SVM, used for classification, to classify the beam loss map patterns. In this study we treat all cases as a binary classification problem, namely finding classifying normal (consistent) and abnormal (inconsistent) patterns. The formalization of the Lagrangian in *dual* form, of the soft-margin SVM, based on its derivation from *primal* form in the second chapter:

$$\mathcal{L}_d = \sum_{i=1}^{events} a_i - \frac{1}{2} \sum_{i=1}^{events} \sum_{j=1}^{events} a_i a_j y_i y_j k(\mathbf{x}_i, \mathbf{x}_j) - \frac{1}{2} C < \boldsymbol{\alpha} \cdot \boldsymbol{\alpha} >$$

Which is a quadratic optimization problem for which Sequential Minimal Optimization (SMO) was used. The kernels under comparison are listed below:

Linear Kernel: $k(\mathbf{x}, \mathbf{y}) = < \mathbf{x}, \mathbf{y} >$

Gaussian Kernel: $k(\mathbf{x}, \mathbf{y}) = \exp(-\frac{\|\mathbf{x}-\mathbf{y}\|^2}{2\sigma^2}) = \exp(-\gamma\|\mathbf{x}-\mathbf{y}\|), \gamma > 0$

Events in the scope of this thesis refer to loss map tuples represented by a UTC timestamp.

4.6.1 Implementation scheme

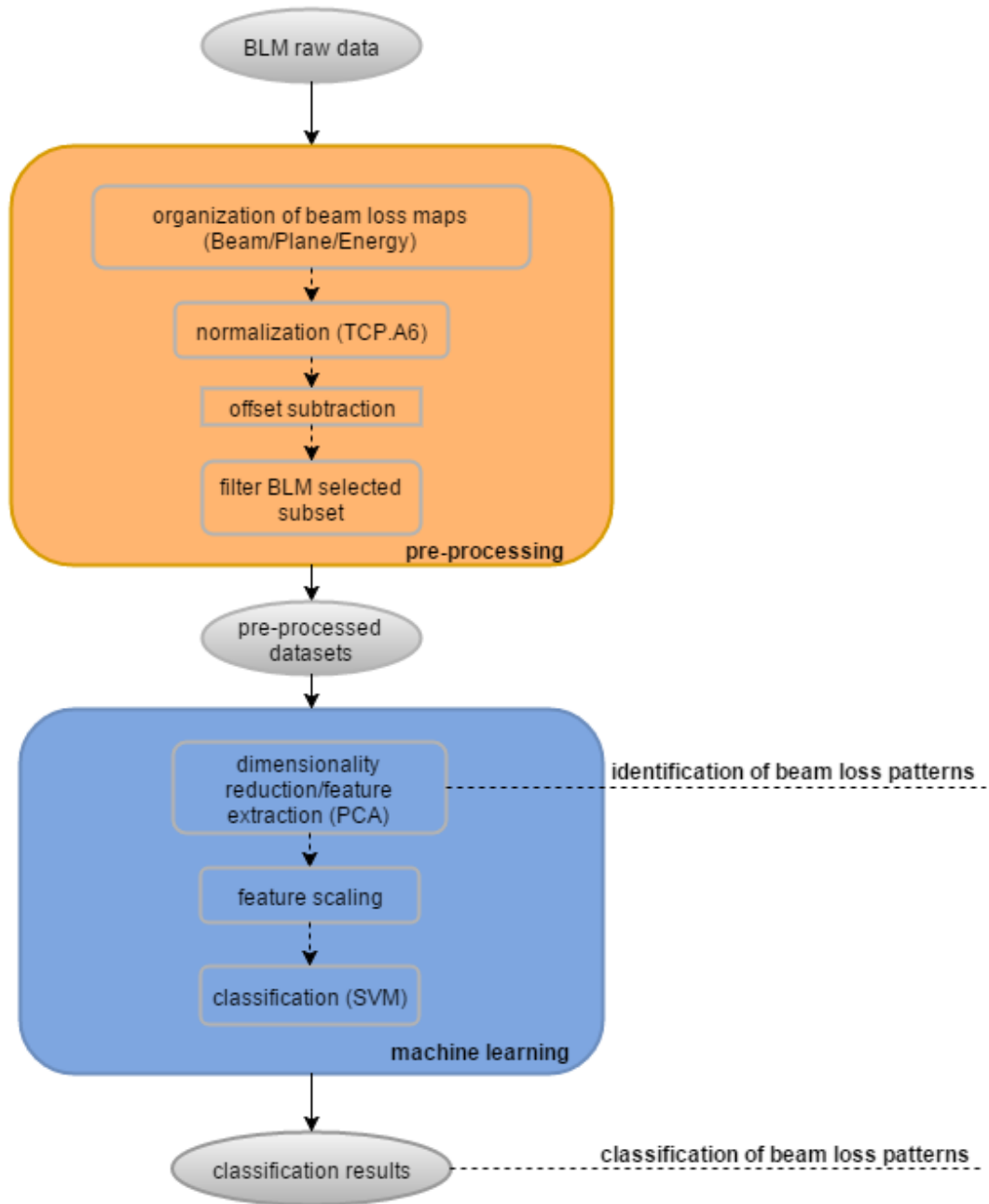


Figure 29: implementation scheme (flowchart)

4.6.2 Model assessment

In statistical learning the models need to be evaluated, in order to quantify their performance based on the given samples. The validation of the model obtained from SVM in this thesis, is done based on the cross-validatory principle [17], for which k-fold cross validation was chosen, partitioning the original samples into k sub-samples which are then used to train the classifier at each one of them. For this reason this evaluation technique can be found being mentioned as rotation estimation as well.

In the second chapter we have presented the exact SVM method used (soft-margin SVM), which requires the determination of the penalty factor C , controlling the slack variables, as well as the optimal parameter γ , which controls the radius of the RBF kernel. The cross validation was included in a scan of parameters C and γ (see Figure 30) the predefined ranges: $range_C = [2^{-10}, 2^{10}]$ and $range_\gamma = [2^{-10}, 2^{10}]$. Then a refined search took place to specify in detail the best combination of C, γ .

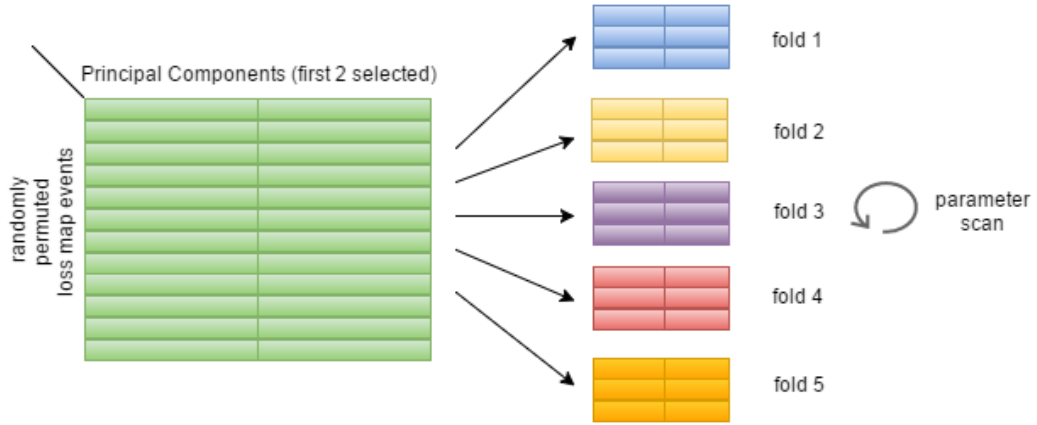


Figure 30: 5-fold cross validation on $\hat{\mathbf{X}}$

The validation took place on a firstly selected subset (validation set) of $\hat{\mathbf{X}}$, independent from the testing set, which originated from setting threshold in the original data set, separating it in the middle. The 5-fold cross-validation was pursued to cross validate the soft-margin SVM on the validation set. A range of success rates from 65% to 100% was retrieved for different combinations of parameters. The best combination found was $C_{best} = 2$ and $\gamma_{best} = 2^{-3.31} \approx 0.01$ for the rbf kernel, which yielded no training error. This was repeated for the reduced data sets $\hat{\mathbf{X}}$ of the remaining case studies, again with no training error after the refined search of parameters.

The performance of the cross validated models per case study - with the concluded parameters C and γ - are tested on the testing samples, per case study (Beam/Plane/Energy), reported in the next section, in classification results.

4.6.3 Classification results

In this section the classification results are presented, focusing in the case of beam loss maps at injection between 2011-2013, including the case study performed in Run II in 2015.

Commencing with the beam loss maps on the horizontal plane of B1, the classification takes place labeling the beam loss patterns of normal or abnormal. In each case the decision boundary corresponding to the linear kernel and rbf (gaussian) kernel is provided. The support vectors are annotated specifically and described in the legend of Figure 31. The training and testing data are also highlighted accordingly.

In particular, since in this case a broken hierarchy was a rare phenomenon (e.g as in Figure 20), the labeling process took into account major and minor abnormalities in the beam loss hierarchy. Thus, we will refer to the two classes as consistent (referring to normal hierarchies) and inconsistent (referring to broken hierarchies and hierarchies with minor abnormalities). In every case representative loss maps are provided to elaborate on the exact location of a beam loss pattern in 2D space.

Figure 31 builds on Figure 23, visualizing the decision boundary separating the good beam loss patterns from the non optimal ones.

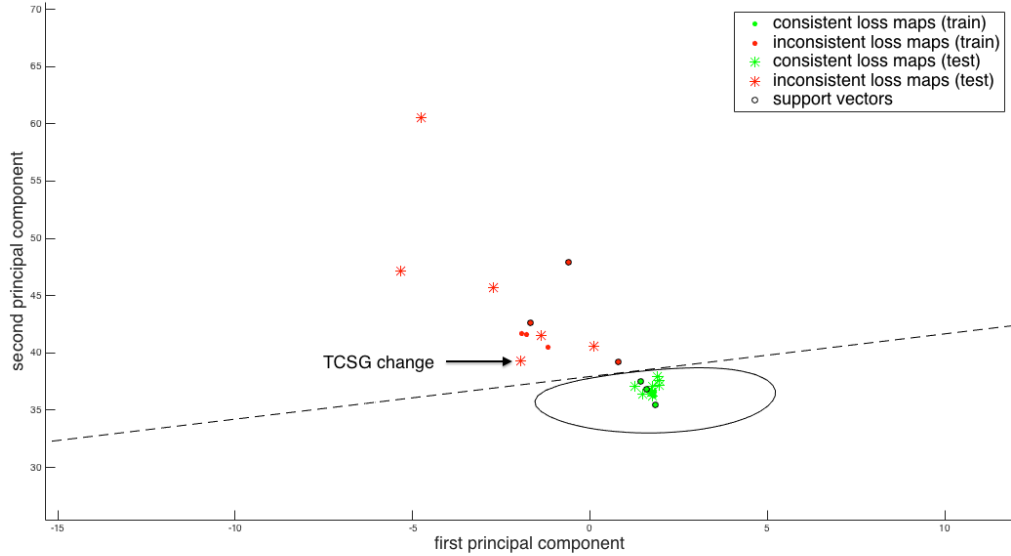


Figure 31: B1HOR450

| linear, rbf | normal (predicted) | abnormal (predicted) |
|-------------------|--------------------|----------------------|
| normal (actual) | 16 (true positive) | 0 (false negative) |
| abnormal (actual) | 0 (false positive) | 13 (true negative) |

Table 13: confusion matrix B1HOR450 (linear, rbf kernel)

Beam loss maps on B1 horizontal with event IDs corresponding to Figure 23 and Table 11.

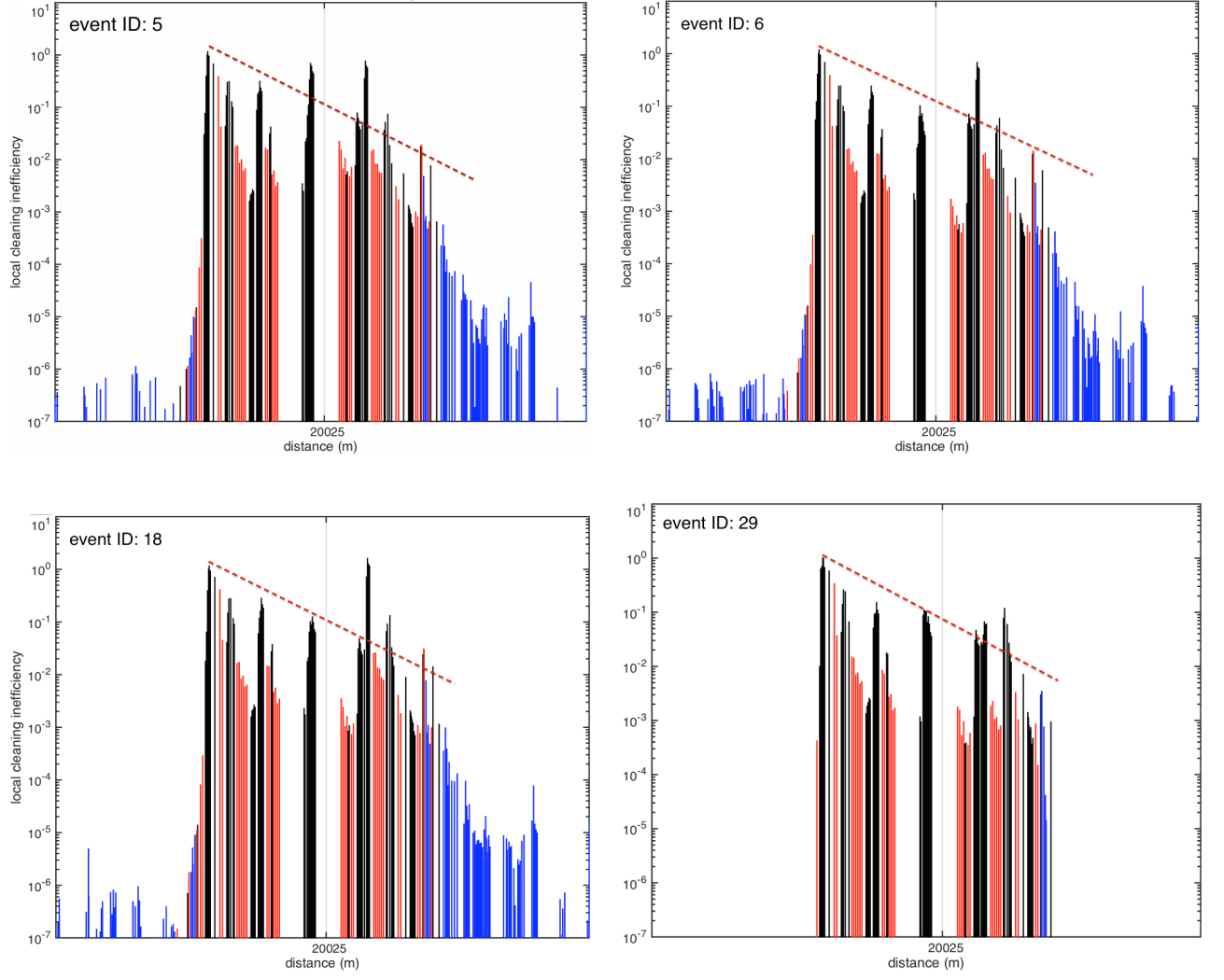


Table 14: abnormal B1HOR450 loss maps

Figure 32 builds on Figure 24 presented earlier in the pattern identification section.

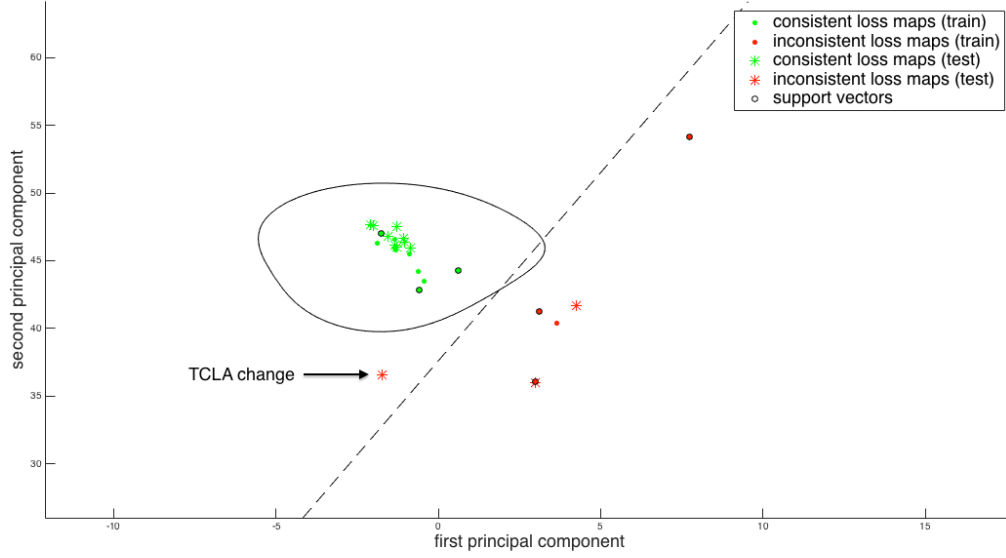


Figure 32: B1VER450

In this particular case the loss map performed in the 2015 test (TCLA setting change) is mis-classified by the linear kernel.

| linear kernel | normal (predicted) | abnormal (predicted) |
|-------------------|--------------------|----------------------|
| normal (actual) | 19 (true positive) | 0 (false negative) |
| abnormal (actual) | 1 (false positive) | 6 (true negative) |

Table 15: confusion matrix B1VER450 (linear kernel)

This results to accuracy 96.16% for the case of the linear kernel on B1 horizontal loss map classification.

| rbf kernel | normal (predicted) | abnormal (predicted) |
|-------------------|--------------------|----------------------|
| normal (actual) | 19 (true positive) | 0 (false negative) |
| abnormal (actual) | 0 (false positive) | 7 (true negative) |

Table 16: confusion matrix B1VER450 (rbf kernel)

In the case of RBF, both classes are classified correctly, obtaining no classification error.

Beam loss maps on B1 vertical with event IDs corresponding to Figure 24 and Table 11.

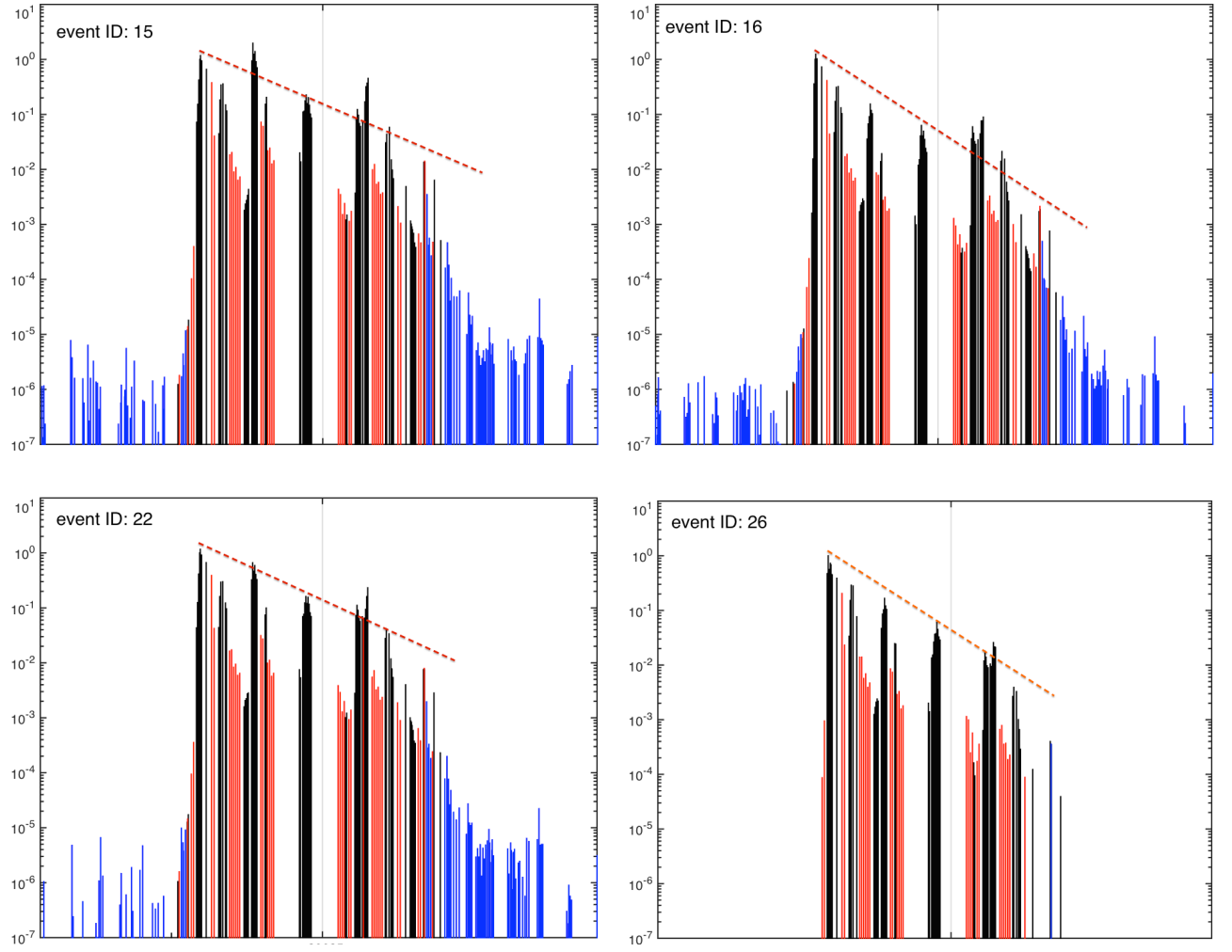


Table 17: abnormal B1VER450 loss maps

Figure 33 builds on Figure 25.

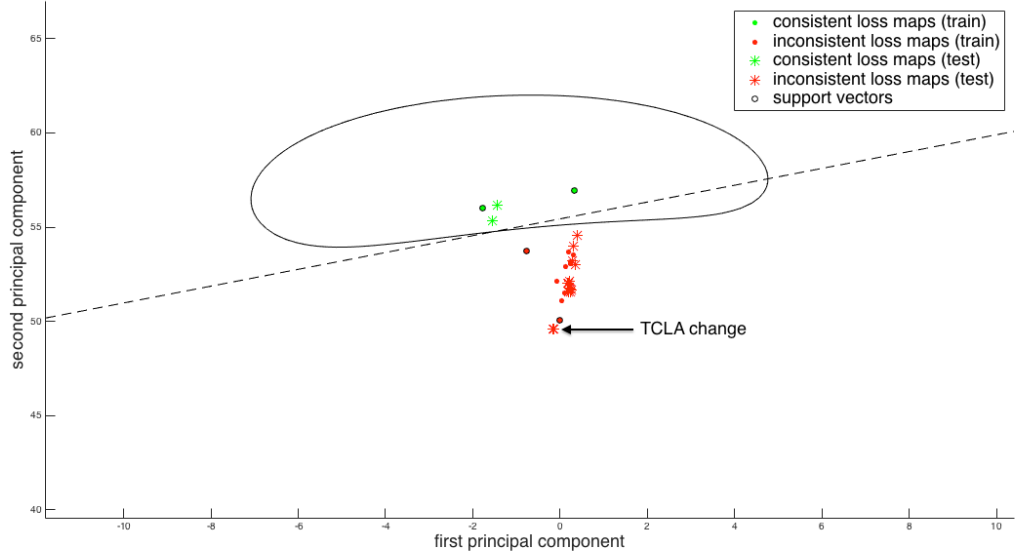


Figure 33: B2HOR450

For beam loss maps on B2 horizontal plane, at injection, the majority of the available measurements contained abnormal hierarchies, resulting to a small subset of loss maps with beam loss patterns that could be labeled as normal (or consistent). This signifies the importance of having a sufficient large number of samples, in order to specify accurately the optimal decision boundary for future data.

| linear, rbf | normal (predicted) | abnormal (predicted) |
|-------------------|--------------------|----------------------|
| normal (actual) | 4 (true positive) | 0 (false negative) |
| abnormal (actual) | 0 (false positive) | 31 (true negative) |

Table 18: confusion matrix B2HOR450 (linear, rbf kernel)

Beam loss maps on B2 horizontal with event IDs corresponding to Figure 25 and Table 11.

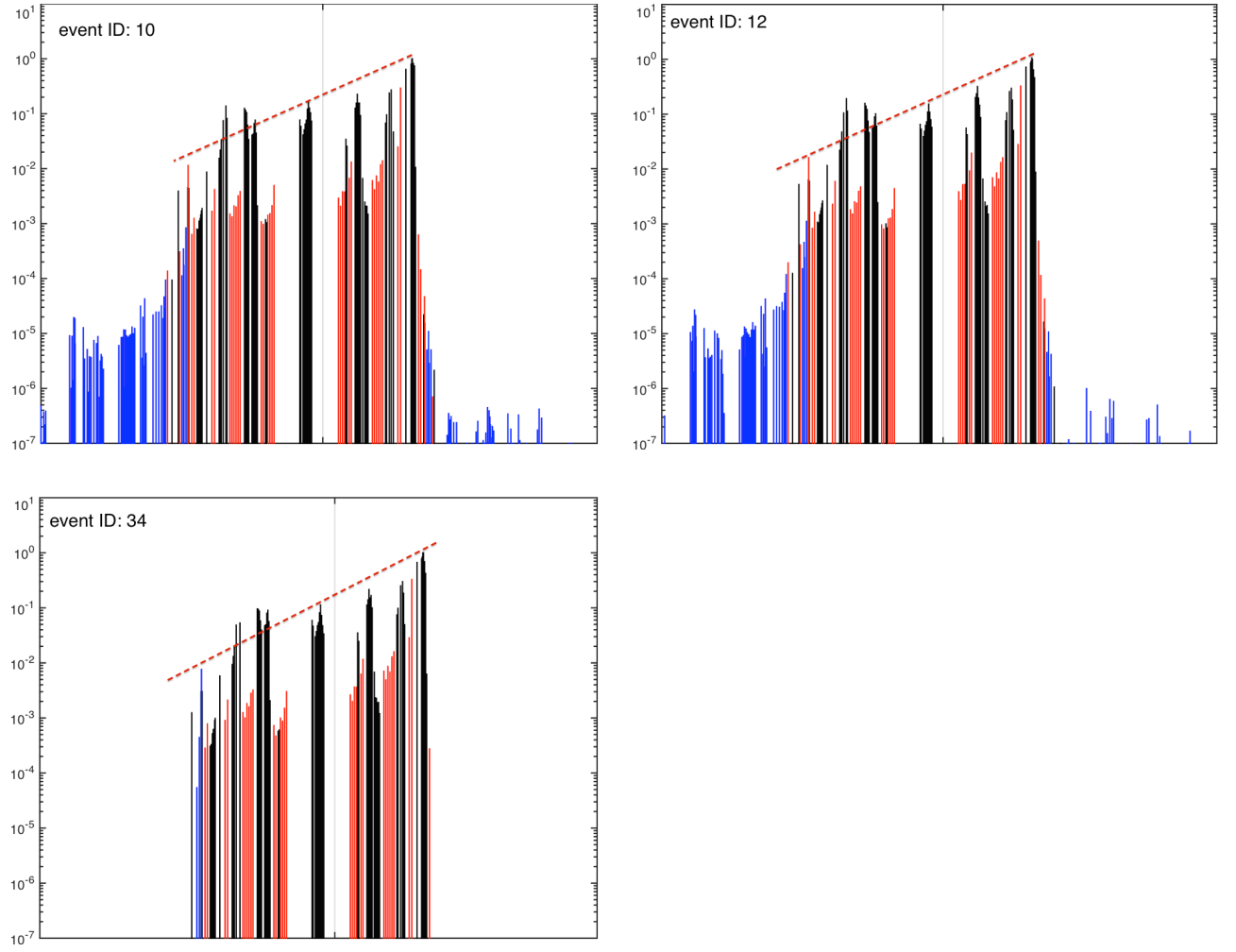


Table 19: abnormal B2HOR450 loss maps

Figure 34 builds on Figure 26.

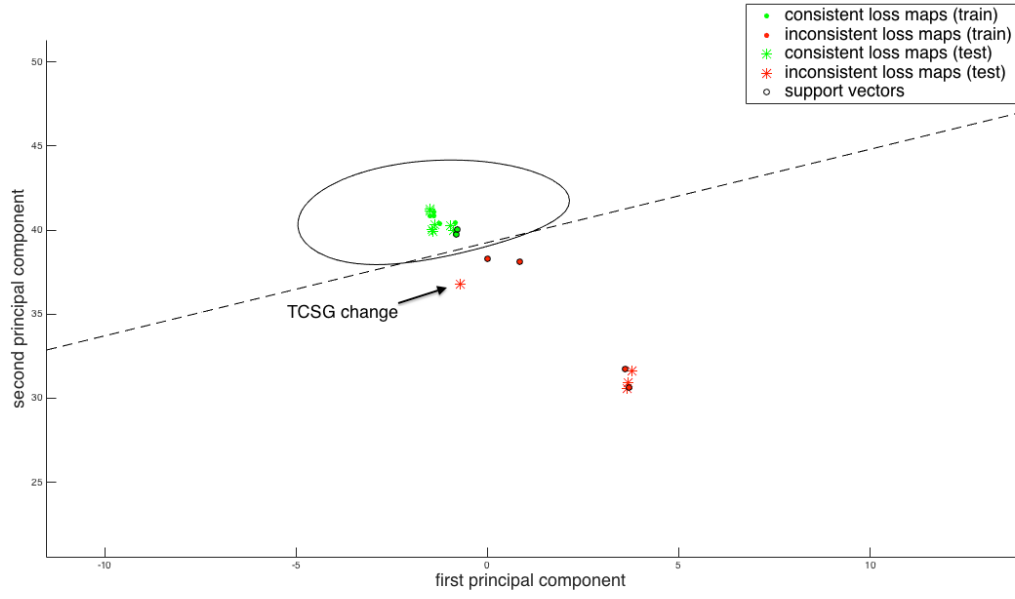


Figure 34: B2VER450

| linear, rbf | normal (predicted) | abnormal (predicted) |
|-------------------|--------------------|----------------------|
| normal (actual) | 14 (true positive) | 0 (false negative) |
| abnormal (actual) | 0 (false positive) | 9 (true negative) |

Table 20: confusion matrix B2VER450 (linear, rbf kernel)

Beam loss maps on B2 vertical with event IDs corresponding to Figure 26 and Table 11.

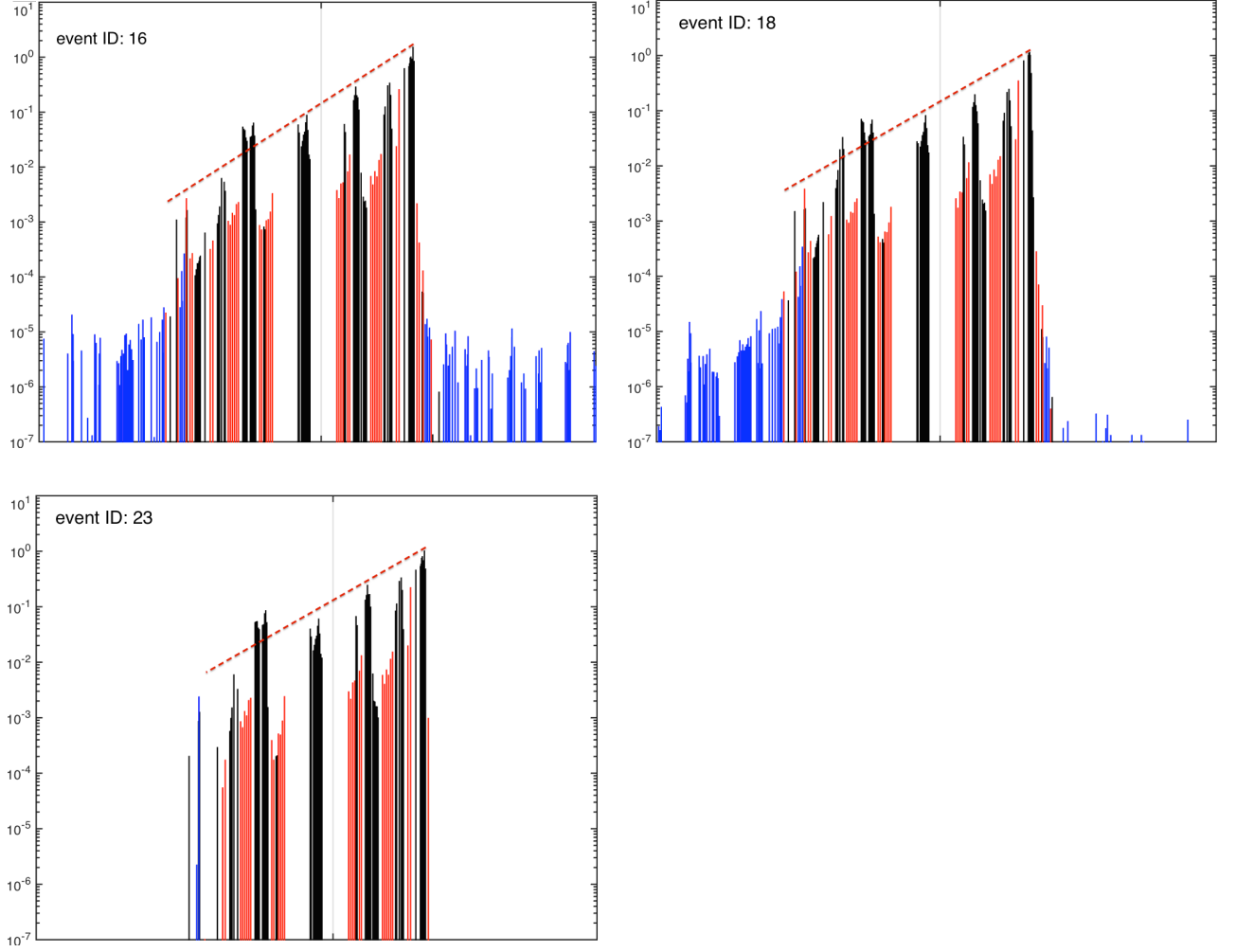


Table 21: abnormal B2VER450 loss maps

The classification of beam loss patterns at injection events (450GeV) for B1HOR, B1VER, B2HOR, B2VER - with addition of 2015 tests - concludes here. Overall, the performance of the proposed method retrieves usable results, being able to visualize multiple beam loss patterns in a 2D space per selected case study (Beam/Plane/Energy). A soft-margin SVM can then be trained to predict occurrence of future beam loss patterns. The downside of the proposed scheme is that the produced model relies heavily on the size of training samples, as well as the exact position of beam loss monitors in the LHC IR7 betatron cleaning hierarchy, as was discussed at the BLM selection section.

5 Conclusion

In this work, standard data analysis steps occurring for evaluating the performance of the LHC collimation system was presented, discussing the main limitations and the necessity of beam loss maps. Physical interpretation of the data sets was elaborated and justified based on characteristics of particle accelerators and in particular of LHC, which have then tailored implementation decisions, such as selection of BLMs, organizing loss maps in case studies per beam properties. Based on that, we have shown that information stored in beam losses, can be maintained at a high level when reducing the dimensionality of the corresponding data sets, verifying also in practice that the patterns observed are meaningful and provide qualitative physical insight. Then a classification scheme was applied, retrieving reliable decision boundaries and discussing downsides of such methods during the evaluation process. The current implementation scheme has potential for use as an application in the CCC to assist in real time evaluation of beam loss maps, which can be also extended to different IRs of LHC, as for example IR3 for the off-momentum cleaning insertion.

References

- [1] D. Achlioptas and F. McSherry. “Fast Computation of Low Rank Approximations”. In: ACM, 2007.
- [2] R. Assmann. “Requirements for the LHC collimation system”. In: *CERN-LHC-Project-Report-599*. 2012.
- [3] R. Bruce et al. “Measurements of heavy ion beam losses from collimation”. In: Phys. Rev. Spec. Top. Accel. Beams 12 (2009).
- [4] O. Brüning et al. *LHCdesignreport*. Tech. rep. 2004.
- [5] H. Burkhardt and R. Schmidt. “Intensity and luminosity after beam scraping”. In: *CERN-AB-2004-032-ABP*.
- [6] C. Cortes and V. Vapnik. “Support Vector Networks”. In: Kluwer Academic Publishers, Boston, 1995.
- [7] A. DasGupta. “Normal Approximations and the Central Limit Theorem”. In: Springer New York, 2010.
- [8] E. B. Holzer et al. “Design of the Beam Loss Monitoring System for the LHC Ring”. In: *EPAC2004*.
- [9] H. Hotelling. “Relations between two sets of variates”. In: Biometrika, 1936.
- [10] A. Lechner et al. “Power deposition in LHC magnets with and without Dispersion Suppressor collimators downstream of the betatron cleaning insertion”. In: IPAC2014.
- [11] A. Masi et al. “LVDT Conditioning on the LHC Collimators”. In: *IEEE Trans. Nucl. Sci.* 55 (2008) 67-75.
- [12] M. E. Mavroforakis and S. Theodoridis. “A Geometric Approach to Support Vector Machine (SVM) classification”. In: IEEE, 2005.
- [13] V. Moens et al. “Comparison of LHC Beam Lossmaps using the transverse dumper blow up and the tune resonance crossing methods”. In: IPAC2013.
- [14] LHC Collimation Project. In: CERN.
- [15] B. Salvachua et al. “Cleaning performance of the LHC collimation system up to 4TeV”. In: IPAC2013.
- [16] B. Schölkopf, A. Smola, and Klaus-Robert Müller. “Kernel Principal Component Analysis”. In: *Advances in kernel methods - support vector learning*. MIT Press, 1999.
- [17] M. Stone. “Cross-Validatory Choice and Assesment of Statistical Predictions”. In: Royal Statistical Society, 1974.
- [18] S. Theodoridis and M. E. Mavroforakis. “Reduced Convex Hulls: A Geometric Approach to Support Vector Machines”. In: IEEE, 2007.
- [19] G. Valentino. “Fast automatic beam based alignment”. In: *CERN-THESIS-2013-208*.
- [20] V. N. Vapnik. *Statistical Learning Theory*. New York: Wiley, 1998.

6 Appendix

6.1 Accelerator Physics

6.1.1 Particle acceleration

Given a particle with mass m and charge q , it is exerted by the Lorentz force, when applying electromagnetic fields $\mathbf{E} = -\nabla\Phi - \frac{\partial\mathbf{A}}{\partial t}$, $\mathbf{B} = \nabla \times \mathbf{A}$ (\mathbf{A} , Φ vector and scalar potential respectively).

$$\frac{d\mathbf{p}}{dt} = \mathbf{F} = q(\mathbf{E} + \mathbf{v} \times \mathbf{B})$$

with momentary velocity $\mathbf{u} = \frac{ds}{dt}$ and mechanical momentum $\mathbf{p} = \gamma m \mathbf{u}$.

$\gamma = \frac{1}{\sqrt{1-\frac{u^2}{c^2}}} = \frac{dt}{d\tau}$ is the relativistic Lorentz factor, with τ *proper time*.

6.1.2 Particle motion

The on-momentum ($\frac{\Delta p}{p} = 0$) linear motion of a particle in an accelerator, is described by the betatron function:

$$x(s) = \sqrt{\epsilon\beta(s)}\cos(\phi(s) + \phi_0)$$

with ϵ the emittance, s referring to the longitudinal displacement along the accelerator, $\beta(s)$ the amplitude modulation due to changing focusing strength $K(s)$ of the quadrupoles and $\phi(s)$ the phase advance.

The betatron function is the solution to Hill's differential equation:

$$\frac{d^2x}{ds^2} + K(s)x = 0$$

which describes a linear harmonic system under the assumption of small oscillations $\sin(x) \approx x$.

6.1.3 Beam scraping

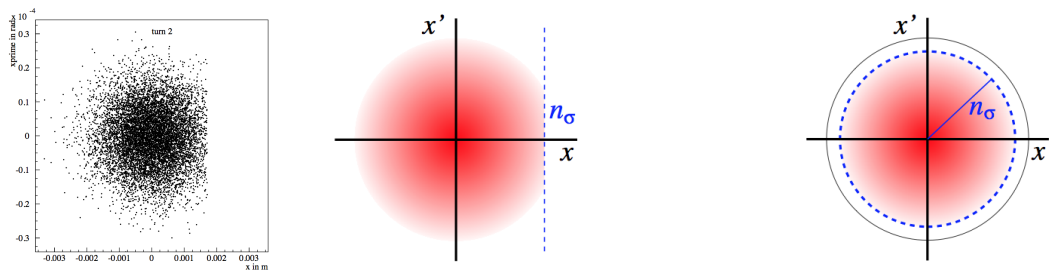


Table 22: beam scraping [5]

6.2 BLM lists

| ID | BLMs (2011 Setup 1) | Loc (m) | ID | BLMs (2011 Setup 1) | Loc (m) |
|----|-------------------------------|---------|----|-------------------------------|---------|
| 1 | BLMEI.07L7.B2I10.TCLA.B7L7.B2 | 19743.6 | 38 | BLMEI.04L7.B1E10.TCSM.A4L7.B1 | 19994.2 |
| 2 | BLMEI.07L7.B2I10.TCLA.A7L7.B2 | 19755.5 | 39 | BLMEI.04R7.B1E10.TCSG.A4R7.B1 | 19996.2 |
| 3 | BLMEI.06L7.B2I10.TCLA.D6L7.B2 | 19773.1 | 40 | BLMEI.04R7.B2I10.TCSM.A4R7.B2 | 19998.2 |
| 4 | BLMEI.06L7.B2I10.TCLA.C6L7.B2 | 19775.1 | 41 | BLMEI.04R7.B1E10.TCSM.A4R7.B1 | 19998.2 |
| 5 | BLMEI.06L7.B1E10.TCP.D6L7.B1 | 19790.2 | 42 | BLMEI.04R7.B2I10.TCSG.A4R7.B2 | 20000.2 |
| 6 | BLMEI.06L7.B1E10.TCP.C6L7.B1 | 19792.2 | 43 | BLMEI.04R7.B2I10.TCSM.B4R7.B2 | 20002.2 |
| 7 | BLMEI.06L7.B1E10.TCP.B6L7.B1 | 19794.2 | 44 | BLMEI.04R7.B2I10.TCSG.B4R7.B2 | 20004.2 |
| 8 | BLMEI.06L7.B1E10.TCP.A6L7.B1 | 19796.2 | 45 | BLMEI.04R7.B2I10.TCSM.D4R7.B2 | 20068.1 |
| 9 | BLMEI.06L7.B1E10.TCHSV.6L7.B1 | 19797.4 | 46 | BLMEI.04R7.B2I10.TCSG.D4R7.B2 | 20070.1 |
| 10 | BLMEI.06L7.B1E10.TCHSH.6L7.B1 | 19798.6 | 47 | BLMEI.05R7.B1E10.TCSM.A5R7.B1 | 20085.4 |
| 11 | BLMEI.06L7.B1E10.TCHSS.6L7.B1 | 19799.8 | 48 | BLMEI.05R7.B1E10.TCSG.B5R7.B1 | 20087.4 |
| 12 | BLMEI.06L7.B2I10.TCLA.B6L7.B2 | 19808.4 | 49 | BLMEI.05R7.B1E10.TCSM.B5R7.B1 | 20089.4 |
| 13 | BLMEI.06L7.B1E10.TCSM.B6L7.B1 | 19831.7 | 50 | BLMEI.05R7.B2I10.TCSM.A5R7.B2 | 20089.4 |
| 14 | BLMEI.06L7.B1E10.TCSG.A6L7.B1 | 19833.7 | 51 | BLMEI.05R7.B2I10.TCSG.A5R7.B2 | 20091.4 |
| 15 | BLMEI.06L7.B1E10.TCSM.A6L7.B1 | 19835.7 | 52 | BLMEI.05R7.B2I10.TCSM.B5R7.B2 | 20093.4 |
| 16 | BLMEI.06L7.B2I10.TCLA.A6L7.B2 | 19839.2 | 53 | BLMEI.05R7.B2I10.TCSG.B5R7.B2 | 20095.4 |
| 17 | BLMEI.06L7.B2I10.TCSM.6L7.B2 | 19844.3 | 54 | BLMEI.05R7.B1E10.TCSG.C5R7.B1 | 20099.4 |
| 18 | BLMEI.06L7.B2I10.TCSG.6L7.B2 | 19846.3 | 55 | BLMEI.05R7.B1E10.TCSG.D5R7.B1 | 20103.4 |
| 19 | BLMEI.05L7.B2I10.TCSM.E5L7.B2 | 19878.9 | 56 | BLMEI.05R7.B1E10.TCSM.D5R7.B1 | 20105.4 |
| 20 | BLMEI.05L7.B2I10.TCSG.E5L7.B2 | 19880.9 | 57 | BLMEI.05R7.B1E10.TCSG.E5R7.B1 | 20107.4 |
| 21 | BLMEI.05L7.B2I10.TCSM.D5L7.B2 | 19882.9 | 58 | BLMEI.05R7.B1E10.TCSM.E5R7.B1 | 20109.4 |
| 22 | BLMEI.05L7.B2I10.TCSG.D5L7.B2 | 19884.9 | 59 | BLMEI.06R7.B1E10.TCSG.6R7.B1 | 20142 |
| 23 | BLMEI.05L7.B2I10.TCSM.C5L7.B2 | 19886.9 | 60 | BLMEI.06R7.B1E10.TCSM.6R7.B1 | 20144 |
| 24 | BLMEI.05L7.B1E10.TCSG.B5L7.B1 | 19892.9 | 61 | BLMEI.06R7.B1E10.TCLA.A6R7.B1 | 20149.1 |
| 25 | BLMEI.05L7.B1E10.TCSM.B5L7.B1 | 19894.9 | 62 | BLMEI.06R7.B2I10.TCSM.A6R7.B2 | 20152.7 |
| 26 | BLMEI.05L7.B1E10.TCSG.A5L7.B1 | 19896.9 | 63 | BLMEI.06R7.B2I10.TCSM.B6R7.B2 | 20156.7 |
| 27 | BLMEI.05L7.B1E10.TCSM.A5L7.B1 | 19898.9 | 64 | BLMEI.06R7.B1E10.TCLA.B6R7.B1 | 20180 |
| 28 | BLMEI.05L7.B2I10.TCSM.B5L7.B2 | 19898.9 | 65 | BLMEI.06R7.B2I10.TCHSH.6R7.B2 | 20189.7 |
| 29 | BLMEI.05L7.B2I10.TCSG.B5L7.B2 | 19900.9 | 66 | BLMEI.06R7.B2I10.TCHSV.6R7.B2 | 20190.9 |
| 30 | BLMEI.05L7.B2I10.TCSM.A5L7.B2 | 19902.9 | 67 | BLMEI.06R7.B2I10.TCP.A6R7.B2 | 20192.1 |
| 31 | BLMEI.04L7.B1E10.TCSG.D4L7.B1 | 19918.2 | 68 | BLMEI.06R7.B2I10.TCP.B6R7.B2 | 20194.1 |
| 32 | BLMEI.04L7.B1E10.TCSM.D4L7.B1 | 19920.2 | 69 | BLMEI.06R7.B2I10.TCP.C6R7.B2 | 20196.1 |
| 33 | BLMEI.04L7.B2I10.TCSM.A4L7.B2 | 19982.2 | 70 | BLMEI.06R7.B2I10.TCP.D6R7.B2 | 20198.1 |
| 34 | BLMEI.04L7.B2I10.TCSG.A4L7.B2 | 19984.2 | 71 | BLMEI.06R7.B1E10.TCLA.C6R7.B1 | 20213.2 |
| 35 | BLMEI.04L7.B1E10.TCSG.B4L7.B1 | 19988.2 | 72 | BLMEI.06R7.B1E10.TCLA.D6R7.B1 | 20215.2 |
| 36 | BLMEI.04L7.B1E10.TCSM.B4L7.B1 | 19990.2 | 73 | BLMEI.07R7.B1E10.TCLA.A7R7.B1 | 20232.9 |
| 37 | BLMEI.04L7.B1E10.TCSG.A4L7.B1 | 19992.2 | 74 | BLMEI.07R7.B1E10.TCLA.B7R7.B1 | 20244.7 |

Table 23: BLM setup 1

| ID | BLMs (2011 Setup 2) | Loc (m) | ID | BLMs (2011 Setup 2) | Loc (m) |
|----|-------------------------------|---------|----|-------------------------------|---------|
| 1 | BLMEI.07L7.B2I10.TCLA.B7L7.B2 | 19743.6 | 39 | BLMEI.04R7.B1E10.TCSG.A4R7.B1 | 19996.2 |
| 2 | BLMEI.07L7.B2I10.TCLA.A7L7.B2 | 19755.5 | 40 | BLMEI.04R7.B1E10.TCSM.A4R7.B1 | 19998.2 |
| 3 | BLMEI.06L7.B2I10.TCLA.D6L7.B2 | 19773.1 | 41 | BLMEI.04R7.B2I10.TCSM.A4R7.B2 | 19998.2 |
| 4 | BLMEI.06L7.B2I10.TCLA.C6L7.B2 | 19775.1 | 42 | BLMEI.04R7.B2I10.TCSG.A4R7.B2 | 20000.2 |
| 5 | BLMEI.06L7.B1E10.TCP.D6L7.B1 | 19790.2 | 43 | BLMEI.04R7.B2I10.TCSM.B4R7.B2 | 20002.2 |
| 6 | BLMEI.06L7.B1E10.TCP.C6L7.B1 | 19792.2 | 44 | BLMEI.04R7.B2I10.TCSG.B4R7.B2 | 20004.2 |
| 7 | BLMEI.06L7.B1E10.TCP.B6L7.B1 | 19794.2 | 45 | BLMEI.04R7.B2I10.TCSM.D4R7.B2 | 20068.1 |
| 8 | BLMEI.06L7.B1E10.TCP.A6L7.B1 | 19796.2 | 46 | BLMEI.04R7.B2I10.TCSG.D4R7.B2 | 20070.1 |
| 9 | BLMEI.06L7.B1E10.TCHSV.6L7.B1 | 19797.4 | 47 | BLMEI.05R7.B1E10.TCSM.A5R7.B1 | 20085.4 |
| 10 | BLMEI.06L7.B1E10.TCHSH.6L7.B1 | 19798.6 | 48 | BLMEI.05R7.B1E10.TCSG.B5R7.B1 | 20087.4 |
| 11 | BLMEI.06L7.B1E10.TCHSS.6L7.B1 | 19799.8 | 49 | BLMEI.05R7.B2I10.TCSM.A5R7.B2 | 20089.4 |
| 12 | BLMEI.06L7.B2I10.TCLA.B6L7.B2 | 19808.4 | 50 | BLMEI.05R7.B1E10.TCSM.B5R7.B1 | 20089.4 |
| 13 | BLMEI.06L7.B1E10.TCSM.B6L7.B1 | 19831.7 | 51 | BLMEI.05R7.B2I10.TCSG.A5R7.B2 | 20091.4 |
| 14 | BLMEI.06L7.B1E10.TCSG.A6L7.B1 | 19833.7 | 52 | BLMEI.05R7.B2I10.TCSM.B5R7.B2 | 20093.4 |
| 15 | BLMEI.06L7.B1E10.TCSM.A6L7.B1 | 19835.7 | 53 | BLMEI.05R7.B2I10.TCSG.B5R7.B2 | 20095.4 |
| 16 | BLMEI.06L7.B2I10.TCLA.A6L7.B2 | 19839.2 | 54 | BLMEI.05R7.B1E10.TCSG.C5R7.B1 | 20099.4 |
| 17 | BLMEI.06L7.B2I10.TCSM.6L7.B2 | 19844.3 | 55 | BLMEI.05R7.B1E10.TCSM.C5R7.B1 | 20101.4 |
| 18 | BLMEI.06L7.B2I10.TCSG.6L7.B2 | 19846.3 | 56 | BLMEI.05R7.B1E10.TCSG.D5R7.B1 | 20103.4 |
| 19 | BLMEI.05L7.B2I10.TCSM.E5L7.B2 | 19878.9 | 57 | BLMEI.05R7.B1E10.TCSM.D5R7.B1 | 20105.4 |
| 20 | BLMEI.05L7.B2I10.TCSG.E5L7.B2 | 19880.9 | 58 | BLMEI.05R7.B1E10.TCSG.E5R7.B1 | 20107.4 |
| 21 | BLMEI.05L7.B2I10.TCSM.D5L7.B2 | 19882.9 | 59 | BLMEI.05R7.B1E10.TCSM.E5R7.B1 | 20109.4 |
| 22 | BLMEI.05L7.B2I10.TCSG.D5L7.B2 | 19884.9 | 60 | BLMEI.06R7.B1E10.TCSG.6R7.B1 | 20142 |
| 23 | BLMEI.05L7.B2I10.TCSM.C5L7.B2 | 19886.9 | 61 | BLMEI.06R7.B1E10.TCSM.6R7.B1 | 20144 |
| 24 | BLMEI.05L7.B1E10.TCSG.B5L7.B1 | 19892.9 | 62 | BLMEI.06R7.B1E10.TCLA.A6R7.B1 | 20149.1 |
| 25 | BLMEI.05L7.B1E10.TCSM.B5L7.B1 | 19894.9 | 63 | BLMEI.06R7.B2I10.TCSM.A6R7.B2 | 20152.7 |
| 26 | BLMEI.05L7.B1E10.TCSG.A5L7.B1 | 19896.9 | 64 | BLMEI.06R7.B2I10.TCSG.A6R7.B2 | 20154.7 |
| 27 | BLMEI.05L7.B2I10.TCSM.B5L7.B2 | 19898.9 | 65 | BLMEI.06R7.B2I10.TCSM.B6R7.B2 | 20156.7 |
| 28 | BLMEI.05L7.B1E10.TCSM.A5L7.B1 | 19898.9 | 66 | BLMEI.06R7.B1E10.TCLA.B6R7.B1 | 20180 |
| 29 | BLMEI.05L7.B2I10.TCSG.B5L7.B2 | 19900.9 | 67 | BLMEI.06R7.B2I10.TCHSS.6R7.B2 | 20188.5 |
| 30 | BLMEI.05L7.B2I10.TCSM.A5L7.B2 | 19902.9 | 68 | BLMEI.06R7.B2I10.TCHSH.6R7.B2 | 20189.7 |
| 31 | BLMEI.04L7.B1E10.TCSG.D4L7.B1 | 19918.2 | 69 | BLMEI.06R7.B2I10.TCHSV.6R7.B2 | 20190.9 |
| 32 | BLMEI.04L7.B1E10.TCSM.D4L7.B1 | 19920.2 | 70 | BLMEI.06R7.B2I10.TCP.A6R7.B2 | 20192.1 |
| 33 | BLMEI.04L7.B2I10.TCSM.A4L7.B2 | 19982.2 | 71 | BLMEI.06R7.B2I10.TCP.B6R7.B2 | 20194.1 |
| 34 | BLMEI.04L7.B2I10.TCSG.A4L7.B2 | 19984.2 | 72 | BLMEI.06R7.B2I10.TCP.C6R7.B2 | 20196.1 |
| 35 | BLMEI.04L7.B1E10.TCSG.B4L7.B1 | 19988.2 | 73 | BLMEI.06R7.B2I10.TCP.D6R7.B2 | 20198.1 |
| 36 | BLMEI.04L7.B1E10.TCSM.B4L7.B1 | 19990.2 | 74 | BLMEI.06R7.B1E10.TCLA.C6R7.B1 | 20213.2 |
| 37 | BLMEI.04L7.B1E10.TCSG.A4L7.B1 | 19992.2 | 75 | BLMEI.06R7.B1E10.TCLA.D6R7.B1 | 20215.2 |
| 38 | BLMEI.04L7.B1E10.TCSM.A4L7.B1 | 19994.2 | 76 | BLMEI.07R7.B1E10.TCLA.A7R7.B1 | 20232.9 |

Table 24: BLM setup 2

| ID | BLMs (2012 Setup 3) | Loc (m) | ID | BLMs (2012 Setup 3) | Loc (m) |
|----|-------------------------------|---------|----|-------------------------------|---------|
| 1 | BLMEI.07L7.B2I10_TCLA.B7L7.B2 | 19743.6 | 39 | BLMEI.04R7.B1E10_TCSG.A4R7.B1 | 19996.2 |
| 2 | BLMEI.07L7.B2I10_TCLA.A7L7.B2 | 19755.5 | 40 | BLMEI.04R7.B1E10_TCSM.A4R7.B1 | 19998.2 |
| 3 | BLMEI.06L7.B2I10_TCLA.D6L7.B2 | 19773.1 | 41 | BLMEI.04R7.B2I10_TCSM.A4R7.B2 | 19998.2 |
| 4 | BLMEI.06L7.B2I10_TCLA.C6L7.B2 | 19775.1 | 42 | BLMEI.04R7.B2I10_TCSG.A4R7.B2 | 20000.2 |
| 5 | BLMEI.06L7.B1E10_TCP.D6L7.B1 | 19790.2 | 43 | BLMEI.04R7.B2I10_TCSM.B4R7.B2 | 20002.2 |
| 6 | BLMEI.06L7.B1E10_TCP.C6L7.B1 | 19792.2 | 44 | BLMEI.04R7.B2I10_TCSG.B4R7.B2 | 20004.2 |
| 7 | BLMEI.06L7.B1E10_TCP.B6L7.B1 | 19794.2 | 45 | BLMEI.04R7.B2I10_TCSM.D4R7.B2 | 20068.1 |
| 8 | BLMEI.06L7.B1E10_TCP.A6L7.B1 | 19796.2 | 46 | BLMEI.04R7.B2I10_TCSG.D4R7.B2 | 20070.1 |
| 9 | BLMEI.06L7.B1E10_TCHSV.6L7.B1 | 19797.4 | 47 | BLMEI.05R7.B1E10_TCSM.A5R7.B1 | 20085.4 |
| 10 | BLMEI.06L7.B1E10_TCHSH.6L7.B1 | 19798.6 | 48 | BLMEI.05R7.B1E10_TCSG.B5R7.B1 | 20087.4 |
| 11 | BLMEI.06L7.B1E10_TCHSS.6L7.B1 | 19799.8 | 49 | BLMEI.05R7.B2I10_TCSM.A5R7.B2 | 20089.4 |
| 12 | BLMEI.06L7.B2I10_TCLA.B6L7.B2 | 19808.4 | 50 | BLMEI.05R7.B1E10_TCSM.B5R7.B1 | 20089.4 |
| 13 | BLMEI.06L7.B1E10_TCSM.B6L7.B1 | 19831.7 | 51 | BLMEI.05R7.B2I10_TCSG.A5R7.B2 | 20091.4 |
| 14 | BLMEI.06L7.B1E10_TCSG.A6L7.B1 | 19833.7 | 52 | BLMEI.05R7.B2I10_TCSM.B5R7.B2 | 20093.4 |
| 15 | BLMEI.06L7.B1E10_TCSM.A6L7.B1 | 19835.7 | 53 | BLMEI.05R7.B2I10_TCSG.B5R7.B2 | 20095.4 |
| 16 | BLMEI.06L7.B2I10_TCLA.A6L7.B2 | 19839.2 | 54 | BLMEI.05R7.B1E10_TCSG.C5R7.B1 | 20099.4 |
| 17 | BLMEI.06L7.B2I10_TCSM.6L7.B2 | 19844.3 | 55 | BLMEI.05R7.B1E10_TCSM.C5R7.B1 | 20101.4 |
| 18 | BLMEI.06L7.B2I10_TCSG.6L7.B2 | 19846.3 | 56 | BLMEI.05R7.B1E10_TCSG.D5R7.B1 | 20103.4 |
| 19 | BLMEI.05L7.B2I10_TCSM.E5L7.B2 | 19878.9 | 57 | BLMEI.05R7.B1E10_TCSM.D5R7.B1 | 20105.4 |
| 20 | BLMEI.05L7.B2I10_TCSG.E5L7.B2 | 19880.9 | 58 | BLMEI.05R7.B1E10_TCSG.E5R7.B1 | 20107.4 |
| 21 | BLMEI.05L7.B2I10_TCSM.D5L7.B2 | 19882.9 | 59 | BLMEI.05R7.B1E10_TCSM.E5R7.B1 | 20109.4 |
| 22 | BLMEI.05L7.B2I10_TCSG.D5L7.B2 | 19884.9 | 60 | BLMEI.06R7.B1E10_TCSG.6R7.B1 | 20142 |
| 23 | BLMEI.05L7.B2I10_TCSM.C5L7.B2 | 19886.9 | 61 | BLMEI.06R7.B1E10_TCSM.6R7.B1 | 20144 |
| 24 | BLMEI.05L7.B1E10_TCSG.B5L7.B1 | 19892.9 | 62 | BLMEI.06R7.B1E10_TCLA.A6R7.B1 | 20149.1 |
| 25 | BLMEI.05L7.B1E10_TCSM.B5L7.B1 | 19894.9 | 63 | BLMEI.06R7.B2I10_TCSM.A6R7.B2 | 20152.7 |
| 26 | BLMEI.05L7.B1E10_TCSG.A5L7.B1 | 19896.9 | 64 | BLMEI.06R7.B2I10_TCSG.A6R7.B2 | 20154.7 |
| 27 | BLMEI.05L7.B2I10_TCSM.B5L7.B2 | 19898.9 | 65 | BLMEI.06R7.B2I10_TCSM.B6R7.B2 | 20156.7 |
| 28 | BLMEI.05L7.B1E10_TCSM.A5L7.B1 | 19898.9 | 66 | BLMEI.06R7.B1E10_TCLA.B6R7.B1 | 20180 |
| 29 | BLMEI.05L7.B2I10_TCSG.B5L7.B2 | 19900.9 | 67 | BLMEI.06R7.B2I10_TCHSS.6R7.B2 | 20188.5 |
| 30 | BLMEI.05L7.B2I10_TCSM.A5L7.B2 | 19902.9 | 68 | BLMEI.06R7.B2I10_TCHSH.6R7.B2 | 20189.7 |
| 31 | BLMEI.04L7.B1E10_TCSG.D4L7.B1 | 19918.2 | 69 | BLMEI.06R7.B2I10_TCHSV.6R7.B2 | 20190.9 |
| 32 | BLMEI.04L7.B1E10_TCSM.D4L7.B1 | 19920.2 | 70 | BLMEI.06R7.B2I10_TCP.A6R7.B2 | 20192.1 |
| 33 | BLMEI.04L7.B2I10_TCSM.A4L7.B2 | 19982.2 | 71 | BLMEI.06R7.B2I10_TCP.B6R7.B2 | 20194.1 |
| 34 | BLMEI.04L7.B2I10_TCSG.A4L7.B2 | 19984.2 | 72 | BLMEI.06R7.B2I10_TCP.C6R7.B2 | 20196.1 |
| 35 | BLMEI.04L7.B1E10_TCSG.B4L7.B1 | 19988.2 | 73 | BLMEI.06R7.B2I10_TCP.D6R7.B2 | 20198.1 |
| 36 | BLMEI.04L7.B1E10_TCSM.B4L7.B1 | 19990.2 | 74 | BLMEI.06R7.B1E10_TCLA.C6R7.B1 | 20213.2 |
| 37 | BLMEI.04L7.B1E10_TCSG.A4L7.B1 | 19992.2 | 75 | BLMEI.06R7.B1E10_TCLA.D6R7.B1 | 20215.2 |
| 38 | BLMEI.04L7.B1E10_TCSM.A4L7.B1 | 19994.2 | 76 | BLMEI.07R7.B1E10_TCLA.A7R7.B1 | 20232.9 |
| | | | 77 | BLMEI.07R7.B1E10_TCLA.B7R7.B1 | 20244.7 |

Table 25: BLM setup 3

| ID | BLMs (2015 Setup 4) | Loc (m) | ID | BLMs (2015 Setup 4) | Loc (m) |
|----|-------------------------------|---------|----|-------------------------------|---------|
| 1 | BLMEI.07L7.B2I10.TCLA.B7L7.B2 | 19743.6 | 43 | BLMTI.04R7.B2I10.TCSG.B4R7.B2 | 20004.2 |
| 2 | BLMTI.07L7.B2I10.TCLA.A7L7.B2 | 19755.5 | 44 | BLMEI.04R7.B2I10.TCSM.D4R7.B2 | 20068.1 |
| 3 | BLMTI.06L7.B2I10.TCLA.D6L7.B2 | 19773.1 | 45 | BLMTI.04R7.B2I10.TCSG.D4R7.B2 | 20070.1 |
| 4 | BLMTI.06L7.B2I10.TCLA.C6L7.B2 | 19775.1 | 46 | BLMEI.05R7.B1E10.TCSM.A5R7.B1 | 20085.4 |
| 5 | BLMTI.06L7.B1E10.TCP.D6L7.B1 | 19790.2 | 47 | BLMTI.05R7.B1E10.TCSG.B5R7.B1 | 20087.4 |
| 6 | BLMTI.06L7.B1E10.TCP.C6L7.B1 | 19792.2 | 48 | BLMEI.05R7.B1E10.TCSM.B5R7.B1 | 20089.4 |
| 7 | BLMTI.06L7.B1E10.TCP.B6L7.B1 | 19794.2 | 49 | BLMEI.05R7.B2I10.TCSM.A5R7.B2 | 20089.4 |
| 8 | BLMEI.06L7.B1E10.TCP.A6L7.B1 | 19796.2 | 50 | BLMTI.05R7.B2I10.TCSG.A5R7.B2 | 20091.4 |
| 9 | BLMEI.06L7.B1E10.TCHSV.6L7.B1 | 19797.4 | 51 | BLMEI.05R7.B2I10.TCSM.B5R7.B2 | 20093.4 |
| 10 | BLMEI.06L7.B1E10.TCHSH.6L7.B1 | 19798.6 | 52 | BLMTI.05R7.B2I10.TCSG.B5R7.B2 | 20095.4 |
| 11 | BLMEI.06L7.B1E10.TCHSS.6L7.B1 | 19799.8 | 53 | BLMEI.05R7.B1E10.TCSG.C5R7.B1 | 20099.4 |
| 12 | BLMTI.06L7.B2I10.TCLA.B6L7.B2 | 19808.4 | 54 | BLMEI.05R7.B1E10.TCSM.C5R7.B1 | 20101.4 |
| 13 | BLMEI.06L7.B1E10.TCSM.B6L7.B1 | 19831.7 | 55 | BLMTI.05R7.B1E10.TCSG.D5R7.B1 | 20103.4 |
| 14 | BLMTI.06L7.B1E10.TCSG.A6L7.B1 | 19833.7 | 56 | BLMEI.05R7.B1E10.TCSM.D5R7.B1 | 20105.4 |
| 15 | BLMEI.06L7.B1E10.TCSM.A6L7.B1 | 19835.7 | 57 | BLMTI.05R7.B1E10.TCSG.E5R7.B1 | 20107.4 |
| 16 | BLMTI.06L7.B2I10.TCLA.A6L7.B2 | 19839.2 | 58 | BLMEI.05R7.B1E10.TCSM.E5R7.B1 | 20109.4 |
| 17 | BLMTI.06L7.B2I10.TCSG.6L7.B2 | 19846.3 | 59 | BLMTI.06R7.B1E10.TCSG.6R7.B1 | 20142 |
| 18 | BLMEI.05L7.B2I10.TCSM.E5L7.B2 | 19878.9 | 60 | BLMEI.06R7.B1E10.TCSM.6R7.B1 | 20144 |
| 19 | BLMTI.05L7.B2I10.TCSG.E5L7.B2 | 19880.9 | 61 | BLMTI.06R7.B1E10.TCLA.A6R7.B1 | 20149.1 |
| 20 | BLMEI.05L7.B2I10.TCSM.D5L7.B2 | 19882.9 | 62 | BLMEI.06R7.B2I10.TCSM.A6R7.B2 | 20152.7 |
| 21 | BLMTI.05L7.B2I10.TCSG.D5L7.B2 | 19884.9 | 63 | BLMTI.06R7.B2I10.TCSG.A6R7.B2 | 20154.7 |
| 22 | BLMEI.05L7.B2I10.TCSM.C5L7.B2 | 19886.9 | 64 | BLMEI.06R7.B2I10.TCSM.B6R7.B2 | 20156.7 |
| 23 | BLMTI.05L7.B1E10.TCSG.B5L7.B1 | 19892.9 | 65 | BLMTI.06R7.B1E10.TCLA.B6R7.B1 | 20180 |
| 24 | BLMEI.05L7.B1E10.TCSM.B5L7.B1 | 19894.9 | 66 | BLMTL.06R7.B1E10.TCLA.B6R7.B1 | 20180 |
| 25 | BLMTI.05L7.B1E10.TCSG.A5L7.B1 | 19896.9 | 67 | BLMEI.06R7.B2I10.TCHSS.6R7.B2 | 20188.5 |
| 26 | BLMEI.05L7.B1E10.TCSM.A5L7.B1 | 19898.9 | 68 | BLMEL.06R7.B2I10.TCHSS.6R7.B2 | 20188.5 |
| 27 | BLMEI.05L7.B2I10.TCSM.B5L7.B2 | 19898.9 | 69 | BLMEL.06R7.B2I10.TCHSH.6R7.B2 | 20189.7 |
| 28 | BLMTI.05L7.B2I10.TCSG.B5L7.B2 | 19900.9 | 70 | BLMEI.06R7.B2I10.TCHSH.6R7.B2 | 20189.7 |
| 29 | BLMEI.05L7.B2I10.TCSM.A5L7.B2 | 19902.9 | 71 | BLMEI.06R7.B2I10.TCHSV.6R7.B2 | 20190.9 |
| 30 | BLMTI.04L7.B1E10.TCSG.D4L7.B1 | 19918.2 | 72 | BLMEL.06R7.B2I10.TCHSV.6R7.B2 | 20190.9 |
| 31 | BLMEI.04L7.B1E10.TCSM.D4L7.B1 | 19920.2 | 73 | BLMEL.06R7.B2I10.TCP.A6R7.B2 | 20192.1 |
| 32 | BLMEI.04L7.B2I10.TCSM.A4L7.B2 | 19982.2 | 74 | BLMEI.06R7.B2I10.TCP.A6R7.B2 | 20192.1 |
| 33 | BLMTI.04L7.B2I10.TCSG.A4L7.B2 | 19984.2 | 75 | BLMTI.06R7.B2I10.TCP.B6R7.B2 | 20194.1 |
| 34 | BLMTI.04L7.B1E10.TCSG.B4L7.B1 | 19988.2 | 76 | BLMTL.06R7.B2I10.TCP.B6R7.B2 | 20194.1 |
| 35 | BLMEI.04L7.B1E10.TCSM.B4L7.B1 | 19990.2 | 77 | BLMTI.06R7.B2I10.TCP.C6R7.B2 | 20196.1 |
| 36 | BLMTI.04L7.B1E10.TCSG.A4L7.B1 | 19992.2 | 78 | BLMTL.06R7.B2I10.TCP.C6R7.B2 | 20196.1 |
| 37 | BLMEI.04L7.B1E10.TCSM.A4L7.B1 | 19994.2 | 79 | BLMTI.06R7.B2I10.TCP.D6R7.B2 | 20198.1 |
| 38 | BLMTI.04R7.B1E10.TCSG.A4R7.B1 | 19996.2 | 80 | BLMTL.06R7.B2I10.TCP.D6R7.B2 | 20198.1 |
| 39 | BLMEI.04R7.B1E10.TCSM.A4R7.B1 | 19998.2 | 81 | BLMTI.06R7.B1E10.TCLA.C6R7.B1 | 20213.2 |
| 40 | BLMEI.04R7.B2I10.TCSM.A4R7.B2 | 19998.2 | 82 | BLMTI.06R7.B1E10.TCLA.D6R7.B1 | 20215.2 |
| 41 | BLMTI.04R7.B2I10.TCSG.A4R7.B2 | 20000.2 | 83 | BLMTI.07R7.B1E10.TCLA.A7R7.B1 | 20232.9 |
| 42 | BLMEI.04R7.B2I10.TCSM.B4R7.B2 | 20002.2 | 84 | BLMEI.07R7.B1E10.TCLA.B7R7.B1 | 20244.7 |

Table 26: BLM setup 4

| ID | Selected BLMs (2011-2015) | Loc (m) | ID | Selected BLMs (2011 - 2015) | Loc (m) |
|----|-------------------------------|---------|----|-------------------------------|---------|
| 1 | BLMEI.07L7.B2I10.TCLA.B7L7.B2 | 19743.6 | 37 | BLMEI.04L7.B1E10.TCSM.A4L7.B1 | 19994.2 |
| 2 | BLMTI.07L7.B2I10.TCLA.A7L7.B2 | 19755.5 | 38 | BLMTI.04R7.B1E10.TCSG.A4R7.B1 | 19996.2 |
| 3 | BLMTI.06L7.B2I10.TCLA.D6L7.B2 | 19773.1 | 39 | BLMEI.04R7.B1E10.TCSM.A4R7.B1 | 19998.2 |
| 4 | BLMTI.06L7.B2I10.TCLA.C6L7.B2 | 19775.1 | 40 | BLMEI.04R7.B2I10.TCSM.A4R7.B2 | 19998.2 |
| 5 | BLMTI.06L7.B1E10.TCP.D6L7.B1 | 19790.2 | 41 | BLMTI.04R7.B2I10.TCSG.A4R7.B2 | 20000.2 |
| 6 | BLMTI.06L7.B1E10.TCP.C6L7.B1 | 19792.2 | 42 | BLMEI.04R7.B2I10.TCSM.B4R7.B2 | 20002.2 |
| 7 | BLMTI.06L7.B1E10.TCP.B6L7.B1 | 19794.2 | 43 | BLMTI.04R7.B2I10.TCSG.B4R7.B2 | 20004.2 |
| 8 | BLMEI.06L7.B1E10.TCP.A6L7.B1 | 19796.2 | 44 | BLMEI.04R7.B2I10.TCSM.D4R7.B2 | 20068.1 |
| 9 | BLMEI.06L7.B1E10.TCHSV.6L7.B1 | 19797.4 | 45 | BLMTI.04R7.B2I10.TCSG.D4R7.B2 | 20070.1 |
| 10 | BLMEI.06L7.B1E10.TCHSH.6L7.B1 | 19798.6 | 46 | BLMEI.05R7.B1E10.TCSM.A5R7.B1 | 20085.4 |
| 11 | BLMEI.06L7.B1E10.TCHSS.6L7.B1 | 19799.8 | 47 | BLMTI.05R7.B1E10.TCSG.B5R7.B1 | 20087.4 |
| 12 | BLMTI.06L7.B2I10.TCLA.B6L7.B2 | 19808.4 | 48 | BLMEI.05R7.B1E10.TCSM.B5R7.B1 | 20089.4 |
| 13 | BLMEI.06L7.B1E10.TCSM.B6L7.B1 | 19831.7 | 49 | BLMEI.05R7.B2I10.TCSM.A5R7.B2 | 20089.4 |
| 14 | BLMTI.06L7.B1E10.TCSG.A6L7.B1 | 19833.7 | 50 | BLMTI.05R7.B2I10.TCSG.A5R7.B2 | 20091.4 |
| 15 | BLMEI.06L7.B1E10.TCSM.A6L7.B1 | 19835.7 | 51 | BLMEI.05R7.B2I10.TCSM.B5R7.B2 | 20093.4 |
| 16 | BLMTI.06L7.B2I10.TCLA.A6L7.B2 | 19839.2 | 52 | BLMTI.05R7.B2I10.TCSG.B5R7.B2 | 20095.4 |
| 17 | BLMTI.06L7.B2I10.TCSG.6L7.B2 | 19846.3 | 53 | BLMEI.05R7.B1E10.TCSG.C5R7.B1 | 20099.4 |
| 18 | BLMEI.05L7.B2I10.TCSM.E5L7.B2 | 19878.9 | 54 | BLMTI.05R7.B1E10.TCSG.D5R7.B1 | 20103.4 |
| 19 | BLMTI.05L7.B2I10.TCSG.E5L7.B2 | 19880.9 | 55 | BLMEI.05R7.B1E10.TCSM.D5R7.B1 | 20105.4 |
| 20 | BLMEI.05L7.B2I10.TCSM.D5L7.B2 | 19882.9 | 56 | BLMTI.05R7.B1E10.TCSG.E5R7.B1 | 20107.4 |
| 21 | BLMTI.05L7.B2I10.TCSG.D5L7.B2 | 19884.9 | 57 | BLMEI.05R7.B1E10.TCSM.E5R7.B1 | 20109.4 |
| 22 | BLMEI.05L7.B2I10.TCSM.C5L7.B2 | 19886.9 | 58 | BLMTI.06R7.B1E10.TCSG.6R7.B1 | 20142 |
| 23 | BLMTI.05L7.B1E10.TCSG.B5L7.B1 | 19892.9 | 59 | BLMEI.06R7.B1E10.TCSM.6R7.B1 | 20144 |
| 24 | BLMEI.05L7.B1E10.TCSM.B5L7.B1 | 19894.9 | 60 | BLMTI.06R7.B1E10.TCLA.A6R7.B1 | 20149.1 |
| 25 | BLMTI.05L7.B1E10.TCSG.A5L7.B1 | 19896.9 | 61 | BLMEI.06R7.B2I10.TCSM.A6R7.B2 | 20152.7 |
| 26 | BLMEI.05L7.B1E10.TCSM.A5L7.B1 | 19898.9 | 62 | BLMEI.06R7.B2I10.TCSM.B6R7.B2 | 20156.7 |
| 27 | BLMEI.05L7.B2I10.TCSM.B5L7.B2 | 19898.9 | 63 | BLMTI.06R7.B1E10.TCLA.B6R7.B1 | 20180 |
| 28 | BLMTI.05L7.B2I10.TCSG.B5L7.B2 | 19900.9 | 64 | BLMEI.06R7.B2I10.TCHSH.6R7.B2 | 20189.7 |
| 29 | BLMEI.05L7.B2I10.TCSM.A5L7.B2 | 19902.9 | 65 | BLMEI.06R7.B2I10.TCHSV.6R7.B2 | 20190.9 |
| 30 | BLMTI.04L7.B1E10.TCSG.D4L7.B1 | 19918.2 | 66 | BLMEI.06R7.B2I10.TCP.A6R7.B2 | 20192.1 |
| 31 | BLMEI.04L7.B1E10.TCSM.D4L7.B1 | 19920.2 | 67 | BLMTI.06R7.B2I10.TCP.B6R7.B2 | 20194.1 |
| 32 | BLMEI.04L7.B2I10.TCSM.A4L7.B2 | 19982.2 | 68 | BLMTI.06R7.B2I10.TCP.C6R7.B2 | 20196.1 |
| 33 | BLMTI.04L7.B2I10.TCSG.A4L7.B2 | 19984.2 | 69 | BLMTI.06R7.B2I10.TCP.D6R7.B2 | 20198.1 |
| 34 | BLMTI.04L7.B1E10.TCSG.B4L7.B1 | 19988.2 | 70 | BLMTI.06R7.B1E10.TCLA.C6R7.B1 | 20213.2 |
| 35 | BLMEI.04L7.B1E10.TCSM.B4L7.B1 | 19990.2 | 71 | BLMTI.06R7.B1E10.TCLA.D6R7.B1 | 20215.2 |
| 36 | BLMTI.04L7.B1E10.TCSG.A4L7.B1 | 19992.2 | 72 | BLMTI.07R7.B1E10.TCLA.A7R7.B1 | 20232.9 |
| | | | 73 | BLMEI.07R7.B1E10.TCLA.B7R7.B1 | 20244.7 |

Table 27: BLM subset selection